HHS Public Access

Author manuscript

Particuology. Author manuscript; available in PMC 2023 May 18.

Published in final edited form as:

Particuology. 2023 January ; 72: 68–80. doi:10.1016/j.partic.2022.02.010.

Computational Fluid Dynamics Simulations of Aerosol Behavior in a High Speed (Heubach) Rotating Drum Dustiness Tester

Hongyu Chen,

Thermal-Fluids and Thermal Processing Lab, Mechanical & Materials Engineering, University of Cincinnati, Cincinnati, OH 45221-0072

Milind A. Jog,

Thermal-Fluids and Thermal Processing Lab, Mechanical & Materials Engineering, University of Cincinnati, Cincinnati, OH 45221-0072

Leonid A Turkevich[*]

Division of Field Studies and Engineering (DFSE), National Institute for Occupational Safety & Health (NIOSH), The Centers for Disease Control & Prevention (CDC), Alice Hamilton Laboratory, 1090 Tusculum Avenue, Cincinnati, OH 45226

Abstract

Potential exposure from hazardous dusts may be assessed by evaluating the dustiness of the powders being handled. Dustiness is the tendency of a powder to aerosolize with a given input of energy. We have previously used computational fluid dynamics (CFD) to numerically investigate the flow inside the European Standard (EN15051) Rotating Drum dustiness tester during its operation. The present work extends those CFD studies to the widely used Heubach Rotating Drum. Air flow characteristics are investigated within the Abe-Kondoh-Nagano k-epsilon turbulence model; the aerosol is incorporated via a Euler-Lagrangian multiphase approach. The air flow inside these drums consists of a well-defined axial jet penetrating relatively quiescent air. The spreading of the Heubach jet results in a fraction of the jet recirculating as back-flow along the drum walls; at high rotation rates, the axial jet becomes unstable. This flow behavior qualitatively differs from the stable EN15051 flow pattern. The aerodynamic instability promotes efficient mixing within the Heubach drum, resulting in higher particle capture efficiencies for particle sizes $d < 80$ μm.

Graphical Abstract

[*]corresponding author: LLT0@cdc.gov.

Video Supplemental Material

Link to videos of 90° Heubach drum: i) air only—(a) ω = 15 rpm; (b) ω = 30 rpm; ii) particle trajectories—(a) d = 1 μm; (b) d = 20 μm; (c) d = 50 μm; (d) d = 100 μm: https://drive.google.com/drive/folders/1fIIV_8u9zbaTWuolA9N5UA-_ZY5SVHd0?usp=sharing

It is an unfortunate artifact of the videos that the vanes on the wall of the drum do not appear to rotate. In the particle trajectory videos, the particle tracks are shown for the previous Δt ~ 3 seconds.

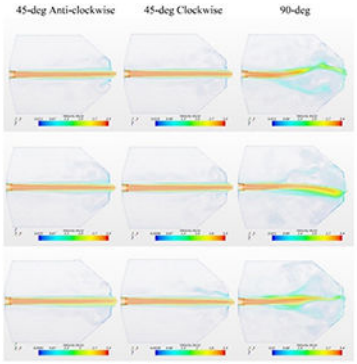

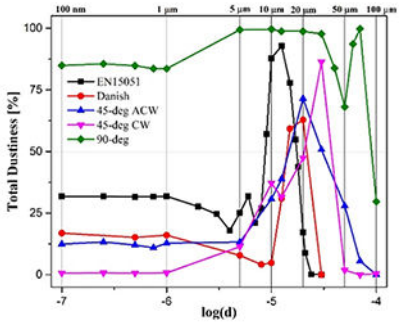

Keywords

Rotating Drum; Dustiness; Euler-Lagrangian Multiphase; AKN k-epsilon Turbulence

1. Introduction

1.1 Dust and Dustiness

1.1.1 Dust—Dust consists of fine and ultrafine solid particles (typically formed by the physical disintegration of a parent material) that may become aerodynamically suspended (Kulkarni, Baron & Willeke, 2011). Outdoor dust is typically generated by natural processes (e.g., aeolian or volcanic) or by pollution. Indoor dust is largely composed of dead skin cells, plant pollen and organic fibers (human hair, animal fur, textile and paper fibers) (van Bronswijk, 1981). In the workplace, airborne dust may be generated by various processes like spills (Sutter, Johnston & Mishima, 2010), pouring or transferring (Chen et al., 2012; Cheng, 1973; Heitbrink, Baron & Willeke, 1992; Shaw et al., 1998), grinding or milling (Pensis et al., 2006). Dust has long been known to have a hazardous effect on human health: da Vinci (Wallace & Hobbs, 2006), Paracelsus (Kelly, 2008), Agricola (Weber, 2002) all warned about the adverse respiratory effects of dust, especially in the mines. Inhalation of industrial dust can lead to asbestosis (Brody, 1997), silicosis (Wagner, 1997; Weisman & Banks, 2003; Leung, Yu & Chen, 2012), byssinosis (Breum ^ Nielsen, 1996), agricultural pneumoconiosis (Schenker et al., 2009) and coal workers' pneumoconiosis (Castranova & Vallyathan, 2000). For recent reviews of the influence of dust on respiratory health, see Duffin et al. (2002, 2007), Sirajuddin & Kanne (2009), Donaldson & Seaton (2012) and Chen et al. (2021). Hence the accurate measurement of dust and its control is the subject of extensive interest (CEN, 2006).

1.1.2 Dustiness—Dustiness is "the propensity of material to generate airborne dust during its handling" (Liden, 2006; Plinke et al., 1995). It is quantified by measuring that portion of a finely divided solid (a powder) that becomes airborne under controlled mechanical or aerodynamic agitation.

1.1.3 Dustiness Testing Methods—Various measures and apparatuses have been developed for dustiness measurement (Kulkarni, Baron & Willeke, 2011; CEN, 2006; Davies et al., 1988; Boundy, Leith & Poulton, 2006; ISO, 2012; ASTM, 1980; DIN, 1999,

2006). The Venturi instrument has been used to test pharmaceutical powders (Boundy, Leith & Poulton, 2006) and fine and ultrafine powders (Evans et al., 2013). In order to evaluate different dustiness testing procedures, we have initiated a research program using Computational Fluid Dynamics to model various dustiness testing apparatuses.

The rotating drum and continuous drop test methods are included in the European standard EN15051 (CEN, 2006) to determine the dustiness in a workplace environment. Schneider & Jensen (2008) used a smaller Danish drum for dustiness testing. The Australian standard rotating drum is used for dustiness measurement of bulk solids (Standards Australia, 2013; Wypych & Mar, 1988). The Heubach dustmeter, which is included in German Standard (DIN, 2006), has also been widely used for occupational dustiness determination (Heitbrink et al., 1990).

1.1.4 Heubach Method—A smaller variant of the (large EN15051) Rotating Drum dustiness tester was introduced earlier, independently in the pigment (Gawol & Adrian, 1983, 1987, 1988) and nutrition (Stauber & Beutel, 1984)communities, where it is called, respectively, the Heubach or Stauber method. As described below, this method uses a smaller drum, which rotates faster and through which air is forced at a higher volumetric flow rate than with the EN 15051 drum. As we will see, these architectural and operational differences alter the aerodynamics and hence the instrument function of this instrument, and this warrants a separate theoretical treatment from our earlier study (Chen et al., 2021)of the instrument function of the EN15051 drum.

The Heubach drum has been incorporated into the German standard for dustiness measurement (DIN, 2006). The Heubach method has been directly compared against the continuous drop method (Heitbrink, 1990; Plinke, Maus & Leith, 1992; Carlson et al., 1992; Bach & Schmidt, 2008). The Heubach method has been used to measure the dust from pigments and colorants (Linde, Buetje & Eitel, 2000; Battersby, 2004) and dust generated from rock mining operations (Petavratzi, 2006; Lowndes & Petavratzi, 2007). The Heubach method has also been used extensively to monitor dust from seeds (Heimbach, 2008; Nikolakis et al., 2009; Nuyttens et al., 2013; Jessop, 2015; Holtz, Hagmeyer & Vullriede, 2015; Nuyttens & Verboven, 2015; Zwertvaeghen et al., 2016; Vernay et al., 2019) with especial application to the risk of agricultural dust drift (Foque et al., 2017; Biocca et al., 2019). It has also found extensive use in the dust evaluation of veterinary and animal foodstuffs (Kliriik, Ferguson & Magruder, 1998; Derrieu et al., 2000; EFSA, 2010, 2012a, b, c, 2013, 2016; Bampidis et al., 2020). Recently, the Heubach method has been considered for the measurement of pharmaceutical dust (Ohta et al., 2014).

1.1.5 Comparison of Heubach and EN15051 Drums—While we defer a detailed discussion of the Heubach architecture to Section 2.1, it is instructive to compare the parameters of the large (EN15051) and smaller (Heubach) drums (Table 1). Each drum consists of a cylinder (diameter d_{bulk} and length l_{bulk}) which tapers at the entrance (over length l_{in} down to diameter d_{in}) and at the exit (over length l_{out} down to diameter d_{out}). Air flows through each drum at a volumetric flow rate Q. Each drum rotates at an angular rotation rate ω.

The superficial velocities may be calculated as $v_{axial} = 4\,Q/\pi\,d^2$. The axial transit times are $t_{transit} \sim l/v_{axial}$. The Reynolds numbers are estimated as $Re \sim v_{axial}\,d/\nu$, where $\nu = 1.48 \times 10^{-5}$ m^2/s is the kinematic viscosity of air. The two drums possess comparable dynamic parameters in the bulk (comparable Re_{bulk}, Re_{rot}, $\omega t_{transit}$). However, while the EN15051 drum has laminar flow at the entrance and exit, due to the constricted entrance, the Heubach entrance flow is borderline turbulent; this necessitates the more sophisticated turbulent air flow modeling. As we shall see, the incoming axial jet becomes unstable, due to the super-imposed rotational flow, and this unstable air jet alters the instrument function.

1.1.6 CFD in dustiness tester research—Computational Fluid Dynamics (CFD) has been used for research of dustiness tester apparatus. Dubey, Ghia & Turkevich (2017) used CFD to investigate the injection and sampling process of Venturi dustiness tester. The aerosolization process has also been investigated using CFD (Palakurthi, 2017). CFD is also a common tool in rotating drum dustiness tester research. Yang, et al. (2008) used CFD to investigate the flow regimes of bulk solids in rotating drum. Wangchai, Hastie & Wypych (2013, 2015, 2016), Wangchai (2017) and Ilic et al. (2016) used CFD-DEM to investigate the aggregation characteristic of bulk solids tumbling in two types of rotating drum dustiness testers.

1.2 Previous modeling work

The Wypych group (Univ. of Wollongong, Australia) have conducted Discrete Element Method (DEM) simulations of the Rotating Drum (Wypych & Mar, 1988; Wangchai, Hastie & Wypych, 2013, 2015, 2016; Wangchai, 2017). These simulations model the behavior of large ($d \sim$ mm) particles tumbling in the drum, in the absence of any air flow. The DEM simulations yield information on size and spatial segregation of particles within the rotating drum but are not appropriate for dust generation and transport (10 nm < d < 100 μm) in the presence of the test air flow. We have previously completed a series of simulations of the low speed EN 15051 rotating drum (Chen et al., 2021).

1.3 Summary of this work

This work represents the first modelling of the Heubach Rotating Drum dustiness test method. In this research, the flow field inside the high-speed (Heubach) rotating dustiness tester is simulated numerically. The higher volumetric flow results in turbulent air flow conditions, and the axial air jet, responsible for the transport of dust particles out of the drum (and onto the collecting media) is found to be unstable; this has consequences for the particle-size dependence of the instrument collection efficiency (the ‘instrument function’) of the Heubach drum. The dustiness, measured under this turbulent air flow, is compared with dustiness measurement under laminar flow (EN 15051 drum). The influence of the shape of inner vanes toward dust generation is also discussed.

2. Numerical Method

We have used STAR-CCM+ as the CFD simulation software in this study. STAR-CCM+ can easily track massive particle trajectories. For a general discussion of modeling turbulent dilute particle-laden flows, see (Curtis & van Wachem, 2004; Chen & Wood, 1985; Tsuji,

Morikawa & Shiomi, 1984; Zhang &Reese, 2001; Crowe, 1998; Schwarzkopf, Crowe & Dutta, 2009).

2.1. Grid generation

The geometry of the Heubach drum is a cylinder, tapered at both inlet and outlet. Dimension parameters of this drum are given in Table 2. While the detailed design of the fins for the commercial Heubach drum is proprietary, we have performed simulations for model drums with several fin architectures, which capture a range of possible fin orientations. In particular, we consider fins oriented normal to the outer drum surface (90° model) and also oriented at a 45° angle with respect to the drum surface. In this latter architecture, the rotation orientation becomes important: for the clockwise orientation (45° CW), the fins push the air tangentially; for the anticlockwise orientation (45° ACW), the fins scoop the air tangentially. We believe the commercial Heubach instrument is intermediate between the 90° and 45° ACW models. Shown in Figure 1 is the Heubach drum with 45° oriented vanes (left) and 90° oriented vanes (right). A different grid is required for each geometry.

Structured grids were generated within Star CCM+; cells are cubes ('trimmed cells') in the bulk of the domain and flattened rectangular prisms at the boundary surface; half of the grid cells are situated in the five layers adjacent to the drum wall. There was no refinement in the axial direction near the entrance and exit into/out of the Rotating Drum volume. The grid rigidly rotates, anchored to the rotating drum wall. The basic grid parameters are listed in Table 3. For the 90° vane geometry, three grids were constructed (surface length = 1.5, 2.0, 2.6 mm) and were used for the grid verification study (section 3.4). For the 45° oriented vane geometry, only the most refined grid (surface length = 1.5 mm) was used. Shown in Figure 2 is the finest (1.5 mm) grid on a mid-section slice perpendicular to the axial direction—45° geometry (left) and 90° geometry (right). Note the refinement near the drum wall and the vanes.

2.2. Numerical Simulation Method (CFD)

2.2.1. Air flow only—no particles—At $Q = 20$ L/min, the nominal airflow Reynolds numbers are Re ~ 2300 at the inlet, 200 in the working section, 1300 at the exit of the drum. The rotation of the drum (with its internal fins) generates a moderate swirl to this axial flow. Based on these Reynolds numbers ($\nu/c_{sound} < 10^{-3}$, where c_{sound} is the velocity of sound in air), the flow is incompressible. We model the turbulent air flow with the low-Re AKN k-ε turbulence formulation (Abe, Kondoh & Nagano, `994, 1005); the AKN k-ε has been evaluated by Goriji et al. (2014), Giannuzzi (2014), Zhang et al. (2019) and Xin & Lei (2015).

The finite volume method (FVM) is used to discretize the governing equations. The discretization of equations and domain, as well as the iterations of discretized equations, are all conducted using commercial FVM solver STAR-CCM+. The convection terms are discretized using second-order Upwind Scheme. The transient terms are discretized by second-order Temporal Scheme. The time step is set at $\Delta t = 0.01$ s, and the simulation is run for $\Delta T = 90$ s; even though the total time of the Heubach dustiness experiment is $\Delta T = 300$ s, $\Delta T = 90$ s is sufficient to achieve steady-state (see Figure 7) and hence determine

the instrument function. The discretized governing equations are solved using the SIMPLE algorithm (Semi-Implicit Method for Pressure Linked Equations). Velocity and pressure under-relaxation factors are 0.8 and 0.2, respectively. Drum rotation is incorporated using rigid body motion of both the boundary and the grid. The solution of the equations was considered to be converged when the scaled residuals for the continuity and momentum equations decreased to 10^{-5} for each time step.

2.2.2. Addition of particles—Particle Tracking—In order to simulate the experiments, the particles are initially distributed uniformly in a band at the bottom along the entire length of the drum. The number of particles in the simulations was N = 10^4 for the dustiness simulations and N = 10^2 for the particle track simulations. Particles are injected at $t = 0$ (using the Star CCM+ Parcel Injector) with an initial upward velocity of $v = 1 \times 10^{-6}$ m/s. The parcel injectors are uniformly distributed at the bottom of the drum. Tracking of massive particles is incorporated via the Lagrangian-Euler Method with two-way coupling between air continuum and dispersed particulate phase. Particle – particle interactions are neglected. For the largest particles (D_p = 100 μm), the volume fraction of the drum occupied by the powder is $\phi \sim N \times 10^{-10}$; if all the particles were to accumulate in one cell (side = 1.5 mm), $\phi \sim N \times 10^{-4}$. Particle agglomeration and breakup are also neglected since aerodynamic shear forces are insufficient to break up agglomerates; however, particle impact on the drum walls may induce breakup, and this has been neglected. Particle – drum wall interaction is modeled as pure elastic collision (i.e. unit coefficient of restitution), so no particles stick to the drum wall.

In the Lagrangian-Euler Method, the motion of each dust particle in the Lagrangian frame is given by:

$$m_p \frac{d\boldsymbol{v}_p}{dt} = F_d + F_p + F_{LS} + m_p g \quad \#(1)$$

where m_p and v_p are the mass and velocity of the particle and g is the gravitational acceleration. The drag force, F_d, and pressure force, F_p, are given below. The drag force (in a direction opposite to the motion of the particle) is given by

$$F_d = \frac{1}{2} C_d \rho A_p v_r^2 \quad (2)$$

where $A_p = (\pi/2)\, D_p^2$ is the particle cross-sectional area, D_p is the particle diameter, ρ is the density of air, and the relative particle-air velocity $\boldsymbol{v_r} = u - \boldsymbol{v_p}$, where u is the local air velocity, $\boldsymbol{v_p}$ is the local particle velocity, and where C_d is the Schiller-Naumann (1933) particle drag coefficient. The pressure gradient force is given by

$$F_p = -V_p \nabla p_{static} \quad (3)$$

where $V_p = (\pi/6)\, D_p^3$ is the particle volume, and ∇p_{static} is the gradient of the static air pressure. There is an additional Safman (1965) lift force, F_{LS}, on each particle, due to shear near the walls.

2.2.3. Two-Way Coupling—We have used two-way coupling for these simulations. A result of our simulations is that the particles remained well-dispersed throughout the drum; the aerosol is thus sufficiently dilute so that one-way coupling is sufficient. However, we wanted to admit the possibility of particles accumulating in a localized region of the drum, in which case, the feedback of the particle motion on the fluid would become important, necessitating two-way coupling.

In two-way coupling, the rate of momentum transfer from the particles back to the continuum air phase is achieved by augmenting the Reynolds-averaged Navier-Stokes equations with a sink term

$$S_v = -\Sigma_n F_d^n \, \delta t_n / \Delta t \tag{4}$$

where the sum is over all particles n in the given cell during the computed time step, F_d^n is the drag force (2) exerted by the fluid on the n^{th} particle, and $\delta t_n/\Delta t$ is the fraction of time that the n^{th} particle spends in the given cell during this time step.

3. Results and Discussion

We first discuss (section 3.1) the general air flow characteristics within the drum. We find that the axial jet in the 90° model becomes unstable and wanders. A measure of the mixing that occurs within the drum models is discussed (section 3.2). The addition of particles allows a modeling of the dustiness of these instruments (section 3.3). The instrument function (dustiness of noninteracting monodisperse particles) is the central result of this study (Figure 7). These Heubach instrument functions are compared with similar results from the EN 15051 and Danish drums. We use the calculated dustiness on various grids to verify the grid independence of our simulations (section 3.4). Finally, we analyze (section 3.5) the particle trajectories (for different particle sizes) to gain a deeper understanding into the variation of dustiness with particle size.

3.1 Air Flow Characteristic

In this section, we examine the air flow in the Heubach drum. Differences in air flow will determine differences in aerosol capture efficiency and hence differences in measured dustiness. Three planes perpendicular to the axial direction are selected to study the air flow in the drums: the midplane (8.3 cm from inlet); a downstream plane (12.9 cm from the inlet), and the outlet plane.

At the axial midplane (Figure 3), for the 45° vane model, both clockwise and anti-clockwise rotations of the drum induce a well-defined angular flow (remark: the 8-fold white ‘star’ in Figure 3 is a graphical artifact of displaying angular vectors on a Cartesian grid). Combined with the axial stream, the overall flow is helical, with the fastest part of the stream near the center. This overall angular flow for these smaller, high rotation rate (Heubach) drums, is qualitatively different from the angular flow for the larger, low rotation rate (EN 15051) drum, where there is no appreciable angular air flow. The radially stratified flow rotates concentrically. This concentric laminar flow is not efficient at transporting particles from the outer wall of the drum towards the central axial stream. However, for the 90° vane geometry,

the flow pattern is significantly different. There is no sign of concentric stratified helical flow; in fact, there is negligible coherent angular flow except at the center. We note that the time evolution for the 45° models is stable, whereas the 90° model exhibits significant temporal variation.

Similar behavior is observed on the downstream plane (Figure 4). Again, both 45° models evince concentric angular flow. However, the instability in the 90° model completely eliminates any average angular flow.

Vortex-shedding from the vanes is observed at the axial midplane for all models, similar to the vortex shedding observed from the vanes in the EN15051 drum. Presumably, the shed vortices travel towards the central jet, where their interaction induces asymmetry to the central air flow. The vortices shed in the 90° model are stronger (and the vane tips are closer to the axial centerline) compared to the 45° models. As these vortices interact with the central jet, they cause the jet to wander, which produces a large recirculating flow and destabilizes the central core flow. At the downstream plane, vortex shedding from the vanes can still be seen for the 45° models; however, for the 90° model, the wandering jet obscures any coherent vortex shedding from the vanes.

Figure 5 shows the magnitude of the velocity at the outlet plane. The velocity is primarily axial and sharply focused to the center (both 45° models) but is distorted and wanders in the 90° model.

The differences in stability of the air flow between the 45° and 90° models is made explicit in a side view of the flow (Figure 6). Shown is the velocity vector in the central plane dividing the drum vertically. For both 45° vane models, the air flows are stable axial straight flows in the central region of the drum from inlet (left) to outlet (right). However, for the 90° model, the high-speed wall rotation destabilizes the axial jet, which wanders in the downstream region. Jet destabilization enhances mixing between peripheral and central regions, which has implications for particle trajectories and, ultimately, for the particle capture at the outlet.

3.2 Mixing Strength

Mixing of the aerosol in the drum is determined by its radial transport. A measure of the mixing strength of the various air flows is an average of the radial velocity. Normalizing by the drum radius, gives a radial mixing rate, f. At a given axial plane, we define the mixing rate as the surface integral of the radial velocity divided by the area, A, of the plane, and the radius, R, of the drum

$$f = \frac{1}{R * A} \int_{plane} v_r * dA \tag{5}$$

We believe that the mixing rate differentiates the dustiness instrument function for the various rotating drum configurations. Figure 7 displays the mixing strength at the axial midplane for the different rotating drums. A higher mixing rate leads to a more efficient

instrument function for the apparatus. Figure 7 demonstrates the relative efficiency of the 90° vane geometry at inducing radial motion within the drum. We will see below its impact on dustiness.

3.3 Dustiness

Figure 8 compares the dustiness (fraction of particles collected at the outlet) among the three Heubach models, European model and Danish model. These simulations have all been conducted for N = 10^4 monodisperse silica particles (ρ = 2.5 g/cm^3). For the same material with same the size dust particle, the different apparatuses evince different dustiness measurement results; i.e. the dustiness measurement depends on the dustiness apparatus. This size dependent variation in the performance of the apparatus represents an instrument function for that apparatus.

For particle diameter d < 1 μm, dustiness is independent of particle size for all 5 models. Of these models, the Heubach 90° model has the highest measured dustiness in this small particle regime. For particles in the diameter range 1 μm < d < 100 μm, the Heubach 90° dustiness remains high (> 90%) until the largest diameters. The other models exhibit highest dustiness for an optimal diameter: d ~ 20 μm (Heubach 45° ACW), d ~ 30 μm (Heubach 45° CW), d ~ 12.5 μm (EN 15051), d ~ 20 μm (Danish drum). All models show a drop-off in instrument function for d > 30 μm.

3.4 Grid Independence Verification

We verify the grid independence of our simulations, using simulations of the 90° Heubach model, rotating at 30 rpm, for 90 seconds, with three successively refined structured grids. The grid parameters are shown in Table 4. We have simulated N = 10^4 particles on each of these grids and recorded the fraction of particles collected at the outlet over the course of the 90 second simulation. The results are shown in Figure 9. There is non-monotonic variation in the dustiness for d < 1 μm (these small particles all follow the air flow), and also for the ‘dip’ at d = 50 μm. Elsewhere, the dustiness curves are independent of grid. The small particle dustiness variation suggests a scant but detectable grid dependence of the air flow simulation; however this grid dependence is insufficient to suppress the 90° small particle dustiness to the values seen for 4the 5° architecture or for the European Drum.

3.5 Particle Track Analysis

In order to better understand the size dependence of the Heubach drum instrument function, it is instructive to examine the behavior of particle trajectories for different sized particles. In the following simulations, the trajectories were accumulated for N = 10^2 particles. In Figures 10-14, the particle tracks are color-coded: blue for times early in the simulation (t ~ 0), green for intermediate times (t ~ 40 sec), yellow (t ~ 70 sec) and red (t ~ 90 sec) for times late in the simulation. Three views, axial (top), side (middle), tilted (bottom) are shown by row; the different models, 45° ACW (left), 45° CW (middle), 90° (right) are shown by column.

Figure 10 shows particle trajectories for very small (d = 100 nm) particles for the 3 different Heubach models. The dustiness values are 12.41% (45° ACW), 0.7% (45° CW), and 84.88% (90°). The 45° CW trajectories never intersect the central axial stream, and hence are not

transported to collection at the exit; late in the simulation, the particle trajectories are confined to an intermediate-radius annular region, split between an upstream ring and a downstream ring. The 45° ACW trajectories exhibit some early penetration to the central region, but later are confined to an outer annulus, located 2/3 of the way down the drum. The 90° trajectories penetrate the central core at early times; there appears to be a residual outer annulus at later times; however, most of the particles have exited the drum by that time.

Figure 11 shows particle trajectories for small (d = 1 μm) particles in the 3 Heubach models. The particle tracks are very similar to the very small (d = 100 nm) tracks shown earlier (Figure 8). The dustiness (fraction of particles collected by 90 seconds) values are 12.42% (45° ACW), 0.75%, (45° CW) and 83.56% (90°), similar to the values for d = 100 nm particles.

Figure 12 shows the particle tracks for intermediate (d = 20 μm) sized particles. The dustiness (fraction of particles collected after 90 seconds) values are significantly higher: 71.48% (45° ACW), 47.35% (45° CW), and 98.75% (90°). In 90° drum (right column), the particles are swept into the central axial stream very early in the simulation and are transported out of the drum. For 45° ACW drum (left column) at early times, the particles circulate in the cylindrical drum at a larger radius compared to the other models; at intermediate times, the trajectories explore smaller radii, and the particles may be swept out of the drum. In 45° CW drum (middle column), at intermediate times, the trajectories explore smaller radii, and the particles may be swept out of the drum.

Figure 13 shows the particle tracks for large (d = 50 μm) particles. The dustiness values are 27.94% (45° ACW), 1.86% (45° CW), and 68.09% (90°). Particle tracks are significantly different from those of the smaller particles. The weight of the particle allows for the trajectory to detach and fall away from the rotating drum wall. Particles escape the drum only if the trajectory intersects the central air flow. In all three models, the particles that fail to escape are trapped in circulation between vanes. This gravity-driven particle falling and recirculation within the Heubach drum is very similar to the large particle trajectories for the EN 15051 drum [Chen 2021].

Figure 14 shows the trajectories for the very large (d = 100 μm) particles. The dustiness values are 0.7% (45° ACW), 0.43% (45° CW), and 29.67% (90°). The behavior is very similar to that observed for the d = 50 μm particles.

4. Conclusion

Potential exposure from hazardous dusts may be assessed by evaluating the dustiness of the powders being handled. Dustiness is the tendency of a powder to aerosolize with a given input of energy. Various techniques are being used to measure dustiness. Much contemporary research attempts to relate the dustiness measurement to the physico-chemical properties of the powder. However, it is important to separate out contributions to dustiness due to materials parameters versus those due to measurement technique. The instrument function, the efficiency of a particular technique at measuring aerosolized powder of a given size, is a measure of the dynamic range of the instrument. The instrument function may

be determined from a CFD simulation of noninteracting particles of that size. As such it separates out the performance of the dustiness measuring instrument from the actual dustiness measured on real powders.

We have previously used computational fluid dynamics (CFD) to simulate the flow inside the Venturi (high Re) and the European Standard (EN15051) Rotating Drum (low Re) dustiness testers during their operation. The present work extended those CFD studies to the widely used Heubach Rotating Drum. As with the larger EN15051 drum, it is found that the Heubach dustiness measurement is sensitive to particle diameter.

Since the air flows within the Heubach drum are turbulent, the CFD modeling is significantly more complicated than the previous modeling of the EN15051 Rotating Drum. Air flow was investigated within the Abe-Kondoh-Nagano k-epsilon turbulence model; the aerosol was incorporated via a Euler-Lagrangian multiphase approach. The air flow inside both the EN15051 and Heubach drums consists of a well-defined axial jet penetrating relatively quiescent air. The spreading of the Heubach jet results in a fraction of the jet recirculating as back-flow along the drum walls; at high rotation rates, the axial jet becomes unstable. This flow behavior qualitatively differs from the stable EN15051 flow pattern. Details of the aerodynamic instability in the Heubach Drum depend on details of the vane geometry and rotation orientation. The aerodynamic instability promotes efficient mixing within the Heubach drum, resulting in higher particle capture efficiencies for particle sizes $d < 80$ μm. Mixing rate (the radius-normalized average of radial velocity) plays a key role in determining the efficiency of the dustiness instrument. A higher mixing rate promotes particle trajectories exploring all radii; this enhances the probability that any given particle trajectory encounters the axial jet and is swept out of the drum. Dustiness of small particles ($d < 1$ μm) is suppressed within both EN15051 and Heubach drums.

Since this work is focused on the instrument function (the particle-size dependence of the instrument collection efficiency) of the Heubach drum, the formation and breakup of agglomerates of smaller size particles were not incorporated into our simulations; similarly, particle adherence to the drum walls was also neglected. The CFD model overpredicts typical experimental dustiness measurements. Experimental powders invariably consist of agglomerates; these larger structures are not aerosolized and are not captured at the outlet—hence, they do not contribute to the measured dustiness. Clearly, agglomeration processes need to be included in simulations of the dustiness of real powder materials.

Supplementary Material

Refer to Web version on PubMed Central for supplementary material.

Acknowledgments

We thank Leonhard Heubach (Heubach GmbH) for helpful discussions on the architecture of the Heubach drum. This work is supported, in part, by the NIOSH Nanotechnology Research Center (NTRC).

Disclaimer

The findings and conclusions in this paper are those of the authors and do not necessarily represent the views of the National Institute for Occupational Safety and Health. Mention of any product or company name does not constitute

endorsement by the Centers for Disease Control and Prevention. None of the authors has a financial relationship with a commercial entity that has an interest in the subject of this paper.

References

Abe K, Kondoh T & Nagano Y (1994). A new turbulence model for predicting fluid flow and heat transfer in separating and reattaching flows—I. Flow field calculations, Int. J. Heat Mass Transfer, 37, 139–151

Abe K, Kondoh T & Nagano Y (1995). A new turbulence model for predicting fluid flow and heat transfer in separating and reattaching flows—II. Thermal field calculations, Int. J. Heat Mass Transfer, 38, 1467–1481

ASTM (1980). Standard Test Method for Index of Dustiness of Coal and Coke, ASTM Standards 26: ANSI/ASTM D-547-41.

Bach S & Schmidt E (2008). Determining the dustiness of powders--a comparison of the measuring devices, Ann. Occ. Hyg, 52 , 717–725.

Bampidis V, Azimonti G, Bastos MI, Christiansen H, Dusemond B, Kos-Durjava M, Kouba M, Lopez-Aloucy M, Lopez-Puente S, Marcon F, Mong B, Pechova A, Petkova M, Ramos F, Sanz Y, Villa RE, Woietersen R, Bories G, Gropp J, Nobbia C, Liberocenti M & Aquilina G (2020). Scientific opinion on the safety and efficacy of vermiculite as a feed additive for pigs, poultry, bovines, sheep, goats, rabbits and horses, EFSAJ, 18, 6160–6169.

Battersby RV (2004). Dustiness and particle size testing of copper and copper compounds, EBRC report prepared for European Copper Institute (20 November 2004, Hannover, Germany).

Biocca M, Fanigliulo R, Pochi D & Gallo P (2019). Dust drift mitigating devices applied as precision pneumatic seed drills: a mini-review, INMATEH--Agricultural Engineering, 58, 273–284.

Boundy M, Leith D & Polton T (2006). Method to evaluate the dustiness of pharmaceutical powders, Ann. Occup. Hyg, 50, 453–458. [PubMed: 16484334]

Breum NO & Nielsen EM (1996). Dust content of cotton-quality control in terms of airborne dust and endotoxin: a pilot study. Gefahrstoffe Reinhaltung Der Luft ,56.10, 389–392.

Brody AR (1997). Asbestosis, in: Roth RA (ed.) Comprehensive Toxicology (Elsevier Science, New York), Vol. 8, pp. 393–413.

Carlson KH, Herman DR, Marksy TF, Wolff RK & Dorato MA (1992). A comparison of two dustiness evaluation methods, Am. Ind. Hyg. Assoc. J, 58 , 448–454.

Castranova V & Vallyathan V (2000). Silicosis and coal workers' pneumoconiosis, Environ. Health Perspectives, 108 (Suppl 4), 675–84.

CEN (2006). Workplace atmospheres - Measurement of the dustiness of bulk materials - Requirements and reference test methods, 28 pages.

Chen C & Wood P, (1985). A turbulence closure model for dilute gas-particle flows, Canad. J Chem. Eng, 63, 349–360

Chen H, Jog MA, Evans DE & Turkevich LA (2021). Numerical Investigation of Powder Aerosolization in a Rotating Drum Apparatus, Powder Techology, 390, 62–72.

Chen X, Wheeler C, Donohue T, McLean R & Roberts A (2012). Evaluation of dust emissions from conveyor transfer chutes using experimental and CFD simulation, Int. J. Mineral Processing, 110, 101–108.

Cheng L (1973). Formation of airborne-respirable dust at belt conveyor transfer points, Am. Ind. Hyg. Assoc J, 34, 540–546. [PubMed: 4770676]

Crowe C (1998). Turbulence modulation of fluid-particle flows--A basic approach, in: Third Int. Conf. Multiphase Flows, 1998

Curtis JS & B. Van Wachem B (2004). Modeling particle-laden flows: a research outlook, AIChE J, 50, 2638–2645

Davies K, Hammond C, Higman R & Wells A (1988). Progress in dustiness estimation: British occupational hygiene society technology committee working party on dustiness estimation, Ann. Occ. Hyg, 32, 535–544.

Derrieu G, Raynes B, Ascher F & Gardey L (2000). Interet de l'utilisation d'une amoxicilline stabilisee pour la fabrication d'aliments medicamenteux, Revue Med. Vet, 151, 109–117.

DIN (1999). Determination of a parameter for the dust formation of pigments and extenders - Part 2: Dropmethod, DIN 55992-2. pp. 6.

DIN (2006). Determination of a parameter for the dust formation of pigments and extenders - Part 1: Rotation method, DIN 55992-1. pp. 8.

Donaldson K & A. Seaton A (2012).A short history of the toxicology of inhaled particles, Part. Fibre Toxicol, 9, 13–13. [PubMed: 22559156]

Dubey P,Ghia U & Turkevich LA (2017). Computational Fluid Dynamics Analysis of the Venturi Dustiness Tester, Powder Technology, 312, 310–320. [PubMed: 28638167]

Duffin R, Tran CL, Clouter A, Brown DM, MacNee W, Stone V & Donaldson K (2002). The Importance of Surface Area and Specific Reactivity in the Acute Pulmonary Inflammatory Response to Particles, Ann. Occup. Hyg, 46, 242–245.

Duffin R, Tran L, Brown D,Stone V & Donaldson K (2007). Proinflammogenic Effects of Low-Toxicity and Metal Nanoparticles In Vivo and In Vitro: Highlighting the Role of Particle Surface Area and Surface Reactivity, Inhalation Toxicology, 19, 849–856. [PubMed: 17687716]

EFSA (2010). Panel on Additives and Products or Substances used in Animal Feed (FEEDAP), Scientific opinion on the safety and efficacy of Vitamin B6 as a feed additive for all animal species, EFSAJ, 8, 1917.

EFSA (2012a). Panel on Additives and Products or Substances used in Animal Feed (FEEDAP), Scientific opinion on the safety and efficacy of selenium in the form of organic compounds produced by the selenium-enriched yeast Saccharomyces cerevisiae NCYC R646 (Selemax 1000/2000) as feed additives for all species. EFSAJ, 10, 2778.

EFSA (2012b). Panel on Additives and Products or Substances used in Animal Feed (FEEDAP), Guidance on studies concerning the safety of use of the additive for users/workers, EFSAJ, 10, 2539–2544

EFSA (2012c). Panel on Additives and Products or Substances used in Animal Feed (FEEDAP), Scientific opinion on the safety and efficacy of Ronozyme Rumistar (alpha-amylase) as a feed additive for dairy cows, EFSAJ, 10, 2777

EFSA (2013). Panel on Additives and Products or Substances used in Animal Feed (FEEDAP), Scientific opinion on the safety and efficacy of Vitamin C as a feed additive for animal species, EFSAJ, 11, 3104.

EFSA (2016). Panel on Additives and Products or Substances used in Animal Feed (FEEDAP), Safety and efficacy of manganese compounds (ES) as feed additives for all animal species, EFSAJ, 14, 4395

Evans DE, Turkevich LA, Roettgers CT, Deye GJ & Baron PA (2013). Dustiness of fine and nanoscale powders, Ann. Occup. Hyg, 57, 261–277. [PubMed: 23065675]

Foque D, Beck B, Devarrewaere W, Verboven P & Nuyttens D (2017). Comparing different techniques to assess the risk of dust drift from pesticide coated seeds, Pest Manag. Sci, 73, 1908–1920. [PubMed: 28233456]

Gawol M & Adrian G (1983). Sustainable, dust-free pigment and coloring preparation, procedure for its manufacturing and measuring appliance for same, DK 350585-A (23 December 1983).

Gawol M & Adrian G (1987). Permanently non-dusting pigment and dye preparations, method for producing them, and measuring device therefor, US4702116 (27 October 1987).

Gawol M & Adrian G (1988). Durable non-dusting pigment and dyestuff preparations, process to manufacture them, EP0144940 (9 March 1988).

Giannuzzi M (2014). Low Reynolds turbulence CFD simulation for complex electronic system: an industrial point of view. J. Phys. Conf. Ser, 525, 01200

Gorji S, Seddighi M, Ariyaratne C, Vardy AE, O'Donoghue T, Pokrajac D & He S (2014). A comparative study of turbulence models in a transient channel flow, Computers & Fluids 89, 111–123

Heimbach U (2008). Heubach method to determine the particulate matter of maize seeds treated with insecticides, Julius-Kuehn-Institut for Plant Production in Field crops and Grass Land report (December 2008, Brunswick, Germany).

Heitbrink WA (1990). Factors affecting the Heubach and MRI dustiness tests, Am. Ind. Hyg. Assoc. J, 51, 210–216. [PubMed: 2327331]

Heitbrink WA, Baron PA & Willeke K (1992). An investigation of dust generation by free falling powders, Am. Ind. Hyg. Assoc. J, 53, 617–624. [PubMed: 1456205]

Heitbrink WA, Todd WF, Cooper TC & O'Brien DM (1990). The application of dustiness tests to the prediction of worker dust exposure, Am. Ind. Hyg. Assoc. J, 51, 217–223. [PubMed: 2327332]

Holtz J, Hagmeyer M & Vullriede S (2015). Heubach method is used to determine abrasion potential of seed treatment coatings: coarse non-volatile and volatile dust particles, European Pest Health Forum 2015.

Ilic D, Planner J, Biswas S & Reid S (2016). Revision of AS4156.6—Coal Preparation—Part 6: Determination of Dust/Moisture Relationship for Coal, in: ICBMH 2016 Conference Proceedings (12th International Conference on Bulk Materials Storage, Handling and Transportation, 11-14 July 2016, Darwin, Australia).

ISO (2012). Nanomaterials -- Quantification of nano-object release from powders by generation of aerosols, ISO/TS 12025, pp. 32.

Jessop N (2015). Methods and uses for improved sowing of seeds, US2015/0013221A1 (published 15 January 2015).

Kelly E (2008). Paracelsus the innovator: a challenge to Galenism from 'On the miner's sickness and other miner's diseases'. Univ. Western Ontario Medical J, 78, 70–74.

Kliriik PR, Ferguson TH & Magruder JA (1998). Formulation of Veterinary Dosage Forms (chapter 2), in: Hardee GE & Baggott JD (eds.) Development and Formulation of Veterinary Dosage Forms (2nd edition) *Drugs and Pharmaceutical Sciences* vol. 88 (Marcel Dekker, New York, 1998), pages 145–230.

Kulkarni P, Baron PA & Willeke K (2011). Introduction of aerosol characterization (chapter 1), in: Kulkarni P, Brown PA, Willeke K (eds.) Aerosol Measurement: Principles, Techniques, and Aapplications (John Wiley & Sons, Hoboken, NJ, 2011), p. 5.

Leung CC, Yu ITS & Chen W (2012). Silicosis, Lancet, 379, 2008–2018. [PubMed: 22534002]

Liden G (2006). Dustiness testing of materials handled at workplaces, Ann Occup Hyg, 50, 437–439. [PubMed: 16849593]

Linde G, Buetje K & Eitel M (2000). Inorganic pigment pellets for coloring plastics, lacquers and building materials and a process for the production thereof, US6132505 (2000).

Lowndes T & Petavratzi E (2007). Assessment of the dustiness and the dust liberation mechanism of limestone quarry operation, Chem Eng. Processing Process Intensification (2007)

Nikolakis A, Chappie A, Friessleben R, Neumann P, Schad T, Schmuck R, Schnier H-F, Schnorbach H-J, Schoening R & Maus C (2009). An effective risk management approach to prevent bee damage due to the emission of abraded seed treatment particles during sowing of seeds treated with bee toxic insecticides, Julius-Kuehn-Archiv, 423, 132–148.

Nuyttens D, Devarrewaere W, Verboven P & Foque D (2013). Pesticide-laden dust emission and drift from treated seeds during seed drilling: a revie, Pest Manag. Sci, 69, 564–575. [PubMed: 23456984]

Nuyttens D & P. Verboven P (2015). Dust emission from pesticide treated seeds during seed drilling, Outlooks in Pest Management (October 2015).

Ohta T, Maeda H, Kubota R, Koga A & Terada K (2014). Establishment of powder dustiness evaluation method by dustmeter with small amount of pharmaceutical ingredients, Int. J. Pharmaceutics, 472, 1–6.

Palakurthi NK (2017). Aerodynamics of Particle Detachment from Surfaces: A Numerical Study, MSc. thesis, University of Cincinnati, Department of Mechanical & Materials Engineering.

Pensis I,Mareels J, Dahmann D & Mark D (2010). Comparative evaluation of the dustiness of industrial minerals according to European standard EN 15051, 2006, Ann. Occup. Hyg, 54, 204–216. [PubMed: 19955327]

Petavratzi E (2006). An Assessment of Dust Generation from Ores. Ph.D. thesis, Univ. of Nottingham, School of Chemical Engineering & Mining Engineering (May 2006).

Plinke MAE, Leith D, Boundy MG & Löffler F (1995). Dust generation from handling powders in industry. Am. Ind. Hyg. Assoc. J, 56, 251–257.

Plinke M, Maus R & Leith D (1992). Experimental examination of factors that affect dust generation by using the Heubach and MRI testers, Am. Ind. Hyg. Assoc. J, 53, 325–330. [PubMed: 1609743]

Safman PG (1965). The lift on a small sphere in a slow shear flow, J. Fluid Mechanics, 22, 385–400.

Schenker MB, Pinkerton KE, Mitchell D, Vallyathan V, Elvine-Kreis B & Green FHY (2009). Pneumoconiosis from Agricultural Dust Exposure among Young California Farmworkers, Environ. Health Perspectives, 117, 988–994.

Schneider T & Jensen KA (2008). Combined single-drop and rotating drum dustiness test of fine to nanosize powders using a small drum, Ann. Occup. Hyg, 52, 23–34. [PubMed: 18056087]

Schwarzkopf JD, Crowe CT & Dutta P (2009). Application of a Volume Averaged k-ε Model to Particle-Laden Turbulent Channel Flow, J. Fluids Eng, 131, 101301.

Schiller L & Naumann A (1933). Ueber die grundlegenden Bereichnungen bei der Schweckraftaufbereitung, VDI Zeits. 77, 318–20.

Shaw BW, Buharivala PP, Parnell CB Jr, & Demny MA (1998). Emission factors for grain receiving and feed loading operations at feed mills, Trans. ASAE, 41, 757–765.

Sirajuddin A & Kanne JP (2009). Occupational lung disease, J Thorac. Imaging, 24, 310. [PubMed: 19935227]

Standards Australia (2013). Coal Preparation--Part 6: Determination of Dust/Moistuer Relationship for Coal, AS4156.6.

Stauber D & Beutel R (1984). Determination and control of the dusting potential of food pre-mixes. Fresenius Z. Anal. Chem, 318, 522–524.

Sutter SL, Johnston JW & Mishima J (2010). Investigation of accident-generated aerosols: releases from free fall spills, Am. Ind. Hyg. Assoc. J, 43, 540–543.

Tsuji Y,Morikawa Y & Shiomi H (1984). LDV measurements of an air-solid two-phase flow in a vertical pipe, J. Fluid Mechanics, 139, 417–434

van Bronswijk JEHM (1981). House Dust Biology for Allergists, Acarologists and Mycologists (Zoelmond, 1981).

Vernay C, Castaing J-C, Zhen Z & Vidal T (2019). Biopolymer-based seed coating composition and methods for use, US2019.0150354 (23 May 2019).

Wagner GR (1997). Asbestosis and silicosis, Lancet, 349, 1311–1315. [PubMed: 9142077]

Wangchai S (2017). Experimental and numerical investigations of particle/air flows in dustiness testers, Ph.D. thesis, Univ. Wollongong, Dept. of Mechanical, Materials, Mechatronic and Biomedical Engineering.

Wangchai S, Hastie DB & Wypych PW (2013). The simulation of particle flow mechanisms in dustiness testers, in: 11th International Conference on Bulk Materials Storage, Handling and Transportation Australia: University of Newcastle, 2013.

Wangchai S, Hastie DB & Wypych PW (2015). The investigation of particle flow mechanisms of bulk materials in dustiness testers, Particulate Science and Technology, 34, 241–254.

Wangchai S, Hastie DB & Wypych PW (2016). Particle size segregation of bulk material in dustiness testers via DEM simulation, Particulate Science and Technology, 36, 20–28.

Wallace JM & Hobbs PV (2006). Atmospheric Science: An Introductory Survey, 2nd edition (Elsevier, Amsterdam, 2006).

Weber LW (2002). Georgius Agricola (1494-1555): Scholar, physician, scientist, entrepreneur, diplomat. Toxicol. Sci, 69, 292–294. [PubMed: 12377977]

Weisman DN & Banks DE (2003). Silicosis and coal worker's pneumoconiosis in: Schwarz MJ & King TE Jr. (eds.) Interstitial Lung Disease. 4th ed. (Decker Inc. Hamilton, BC, 2003), pages 391–416.

Wypych P & Mar L (1988). Investigations into the dustiness of bulk materials. Australian Bulk Handling Review, 18, 64–67

Xin N & Lei L (2015). A comparison of low Reynolds number k-ε models, in: 4th International Conference on Computer, Mechatronics, Control and Electronic Engineering (ICCMCEE 2015): 1334–1339.

Yang R, Yu A, McElroy L & Bao J (2008). Numerical simulation of particle dynamics in different flow regimes in a rotating drum, Powder Technology, 188, 170–177.

Zhang C, Bounds CP, Foster L & Uddin M (2019). Turbulence modeling effects on the CFD prediction of flow over a detailed full-scale sedan vehicle, Fluids, 4, 148.

Zhang Y & Reese JM (2001) Particle–gas turbulence interactions in a kinetic theory approach to granular flows, Int. J. Multiphase Flow, 27, 1945–1964

Zwertvaeghen IKA, Foque D, Devarrewaere W, Verboven P & Nuyttens D (2016). Assessment of the abrasion potential of pesticide-treated seeds using the Heubach test, Int. J. Pest Management, 62, 348–359.

Highlights

- CFD simulations are used to characterize the Heubach dustiness drum.
- The efficiency of the drum (‘instrument function’) depends on the orientation of the internal vanes.
- 90°-oriented vanes generate strong swirl that destabilizes the axial jet.
- A destabilized axial jet (90° vane orientation) efficiently entrains small (d < 1 μm) dust particles.

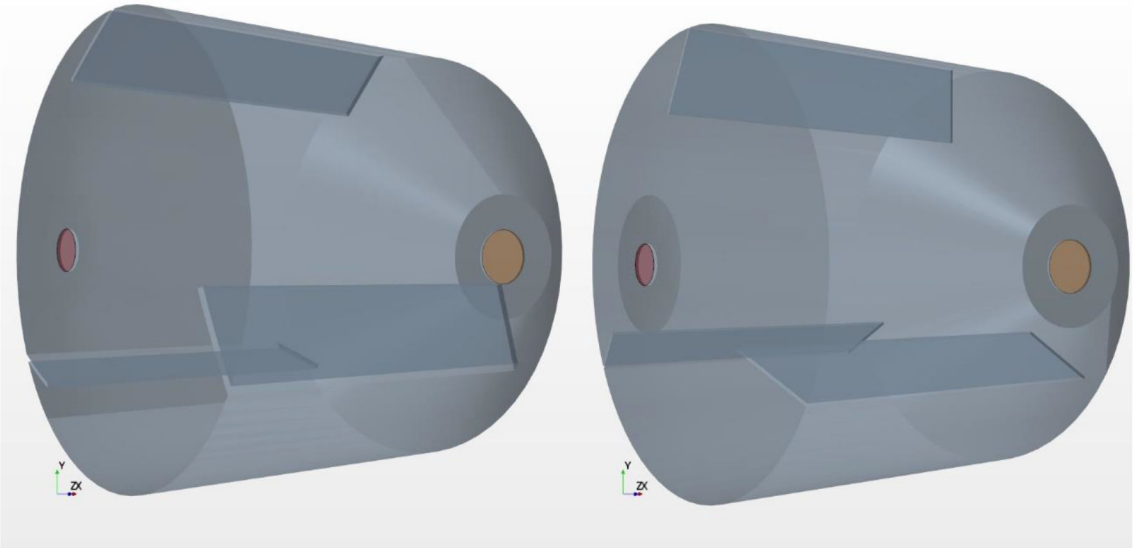

Figure 1.
45° and 90° Heubach Models

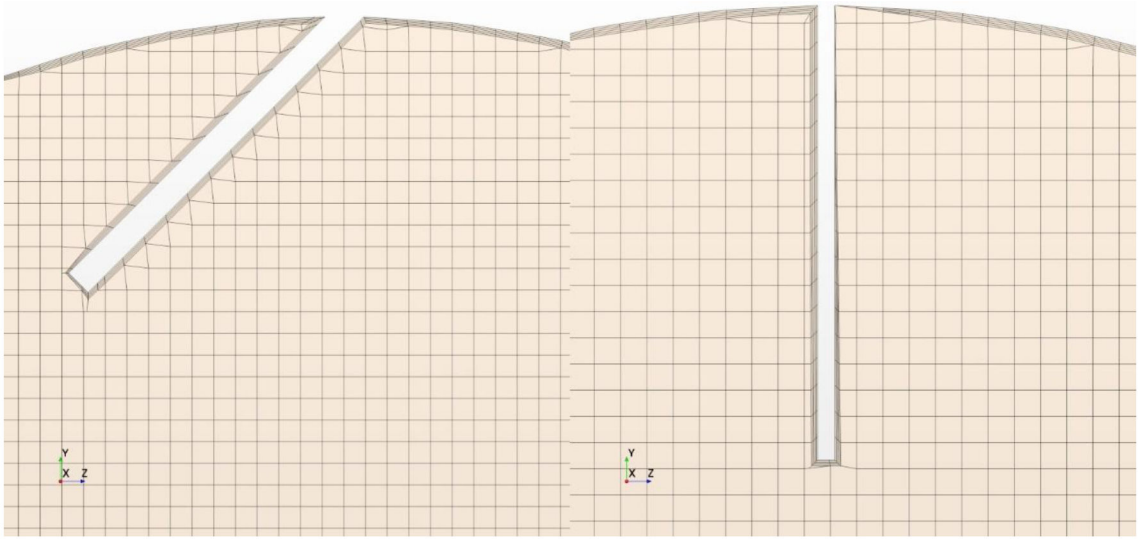

Figure 2.
Meshes of 45° and 90° Heubach Models

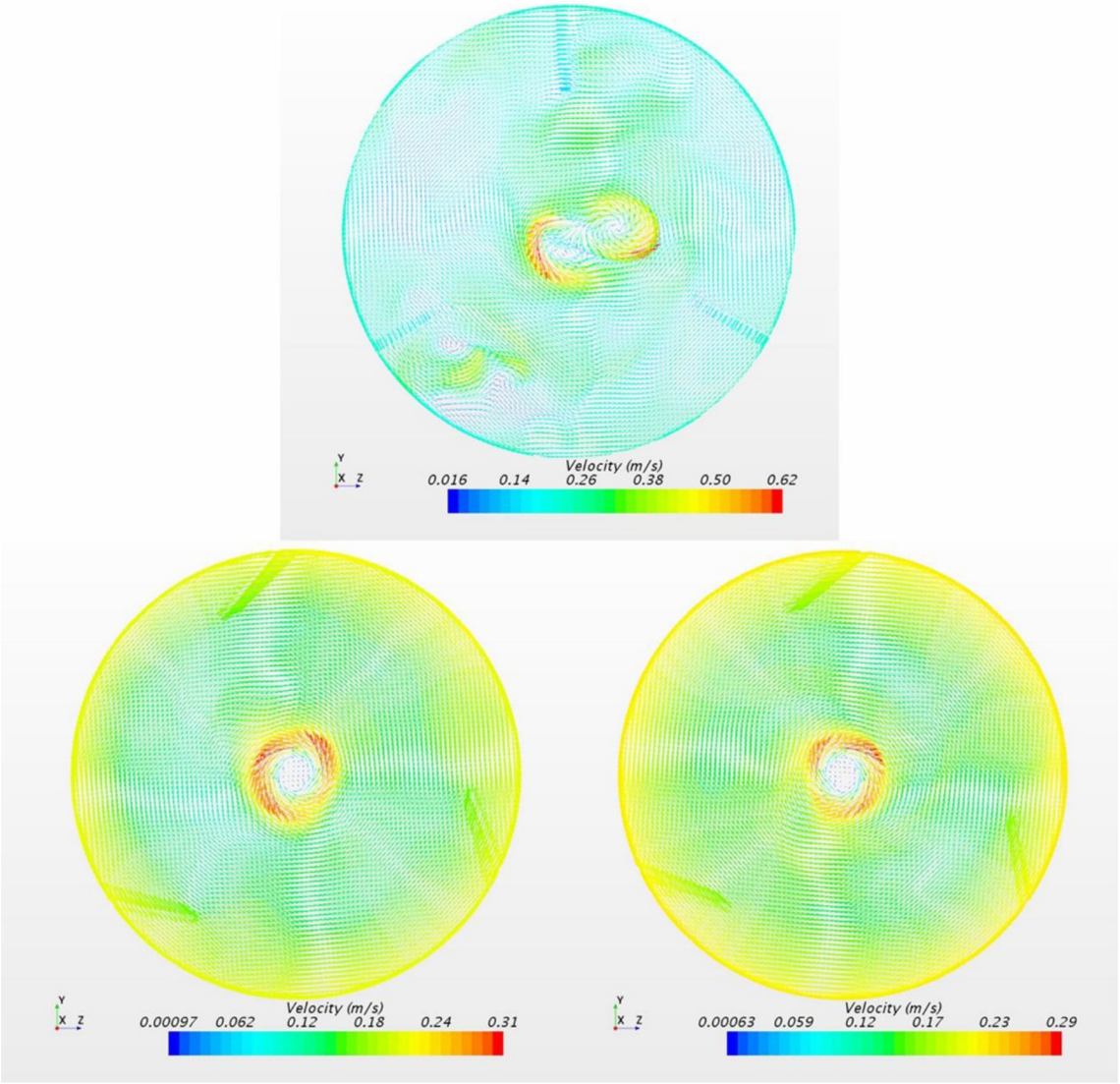

Figure 3a.

Air flow tangential velocity vectors at midplane (8.3 cm) of cylindrical drum (top: 90°; bottom left: 45° anti-clockwise; bottom right: 45° clockwise); t = 30 sec.

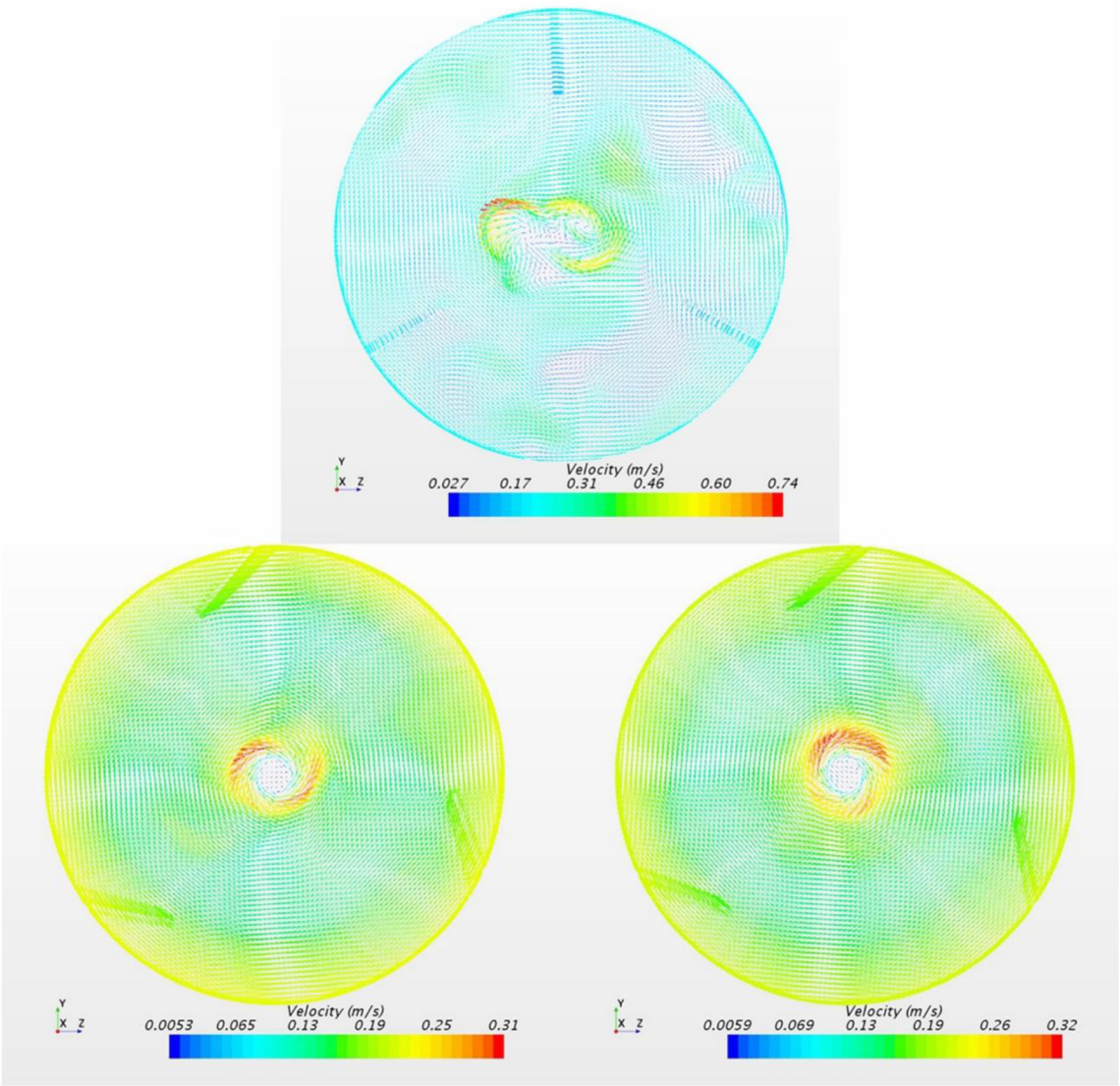

Figure 3b.
Air flow tangential velocity vectors at midplane (8.3 cm) of cylindrical drum (top: 90°; bottom left: 45° anti-clockwise; bottom right: 45° clockwise); t = 60 sec.

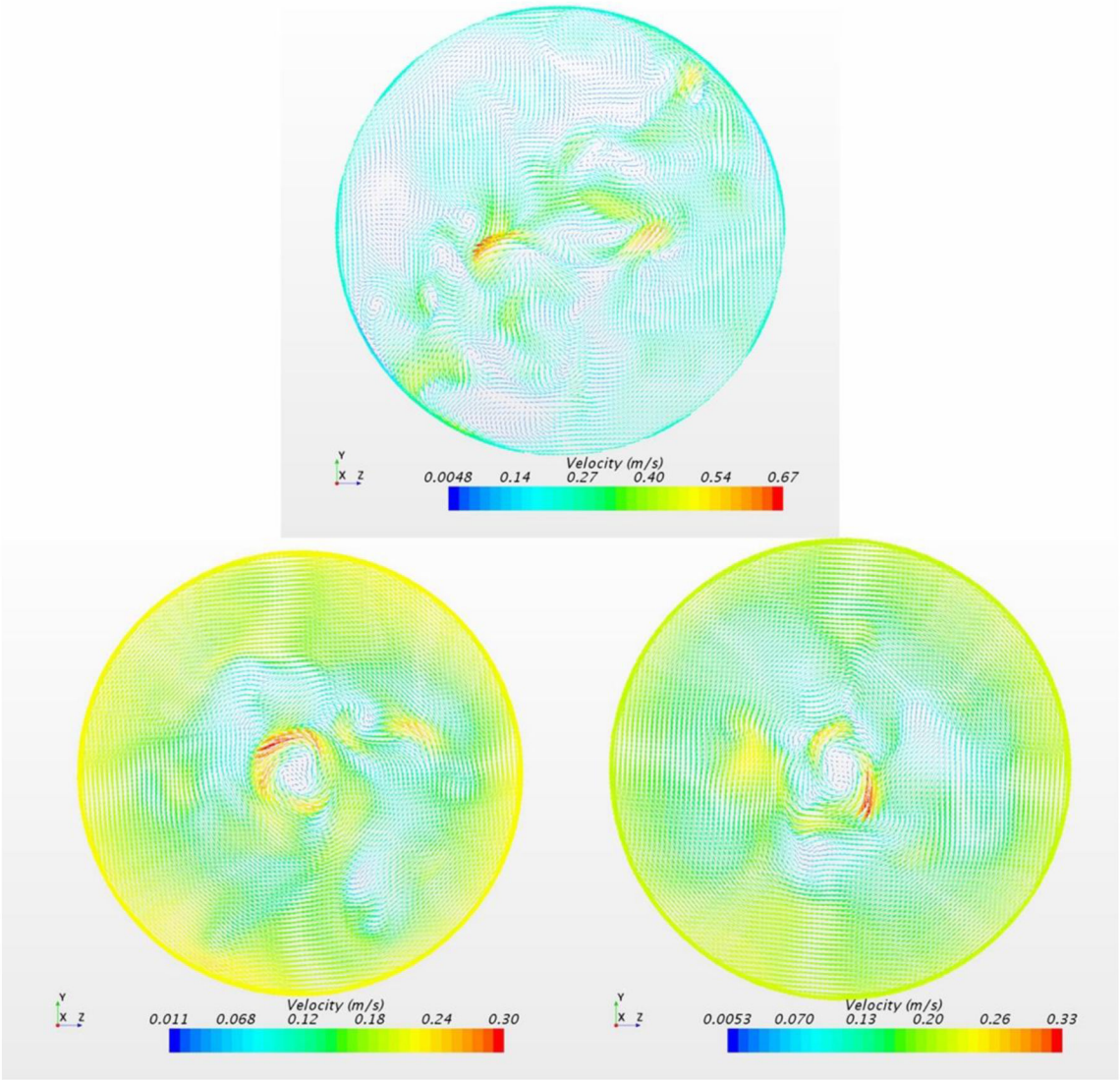

Figure 4a.

Air flow tangential velocity vectors at end plane (12.9 cm) of cylindrical drum (top: 90°; bottom left: 45° anti-clockwise; bottom right: 45° clockwise); t = 30 sec.

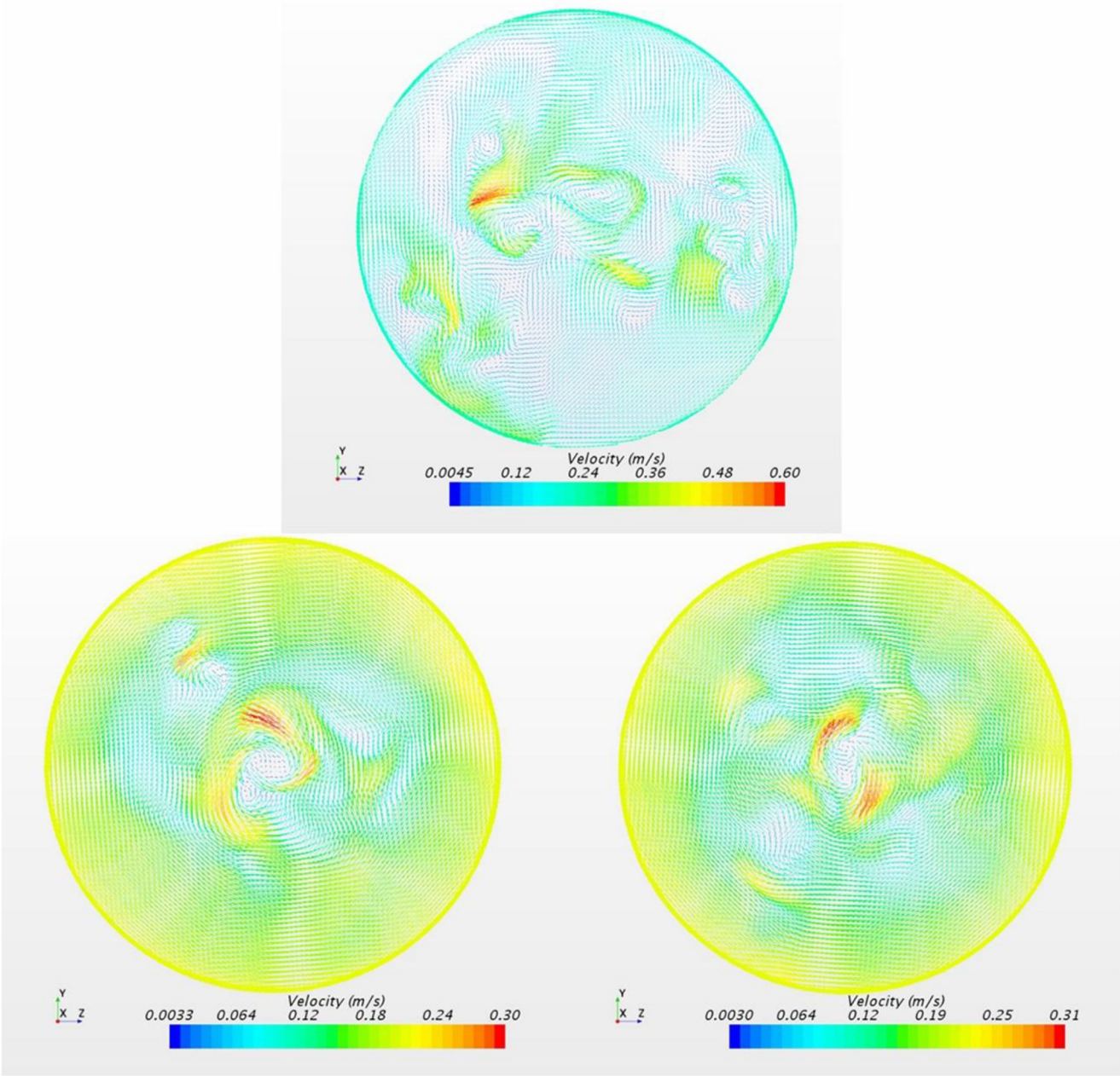

Figure 4b.

Air flow tangential velocity vectors at end plane (12.9 cm) of cylindrical drum (top: 90°; bottom left: 45° anti-clockwise; bottom right: 45° clockwise); t = 60 sec.

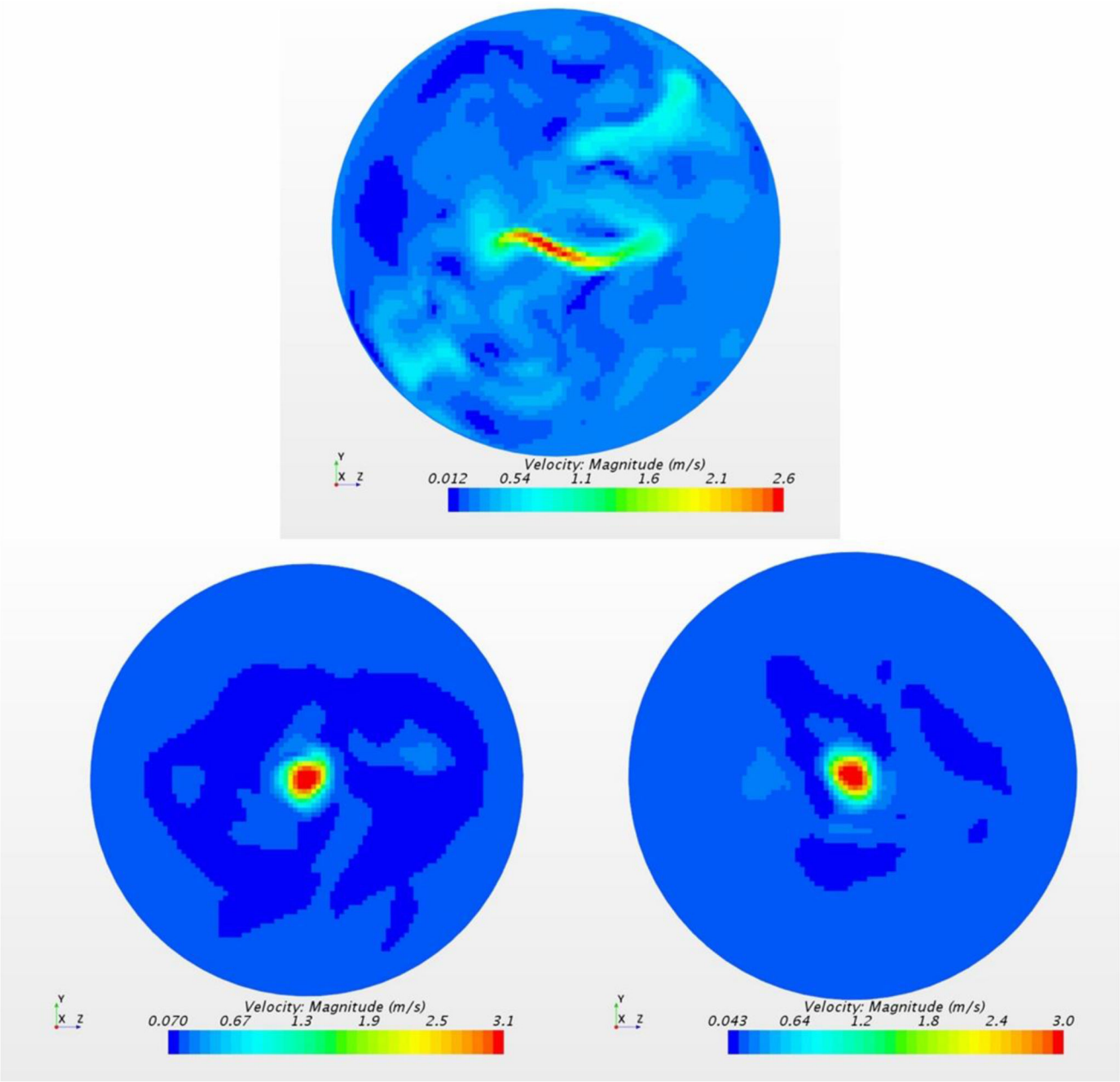

Figure 5a.

Air flow velocity magnitude (cloud image) at end plane (12.9 cm) of cylindrical drum (top: 90°; bottom left: 45° anti-clockwise; bottom right: 45° clockwise); t = 30 sec.

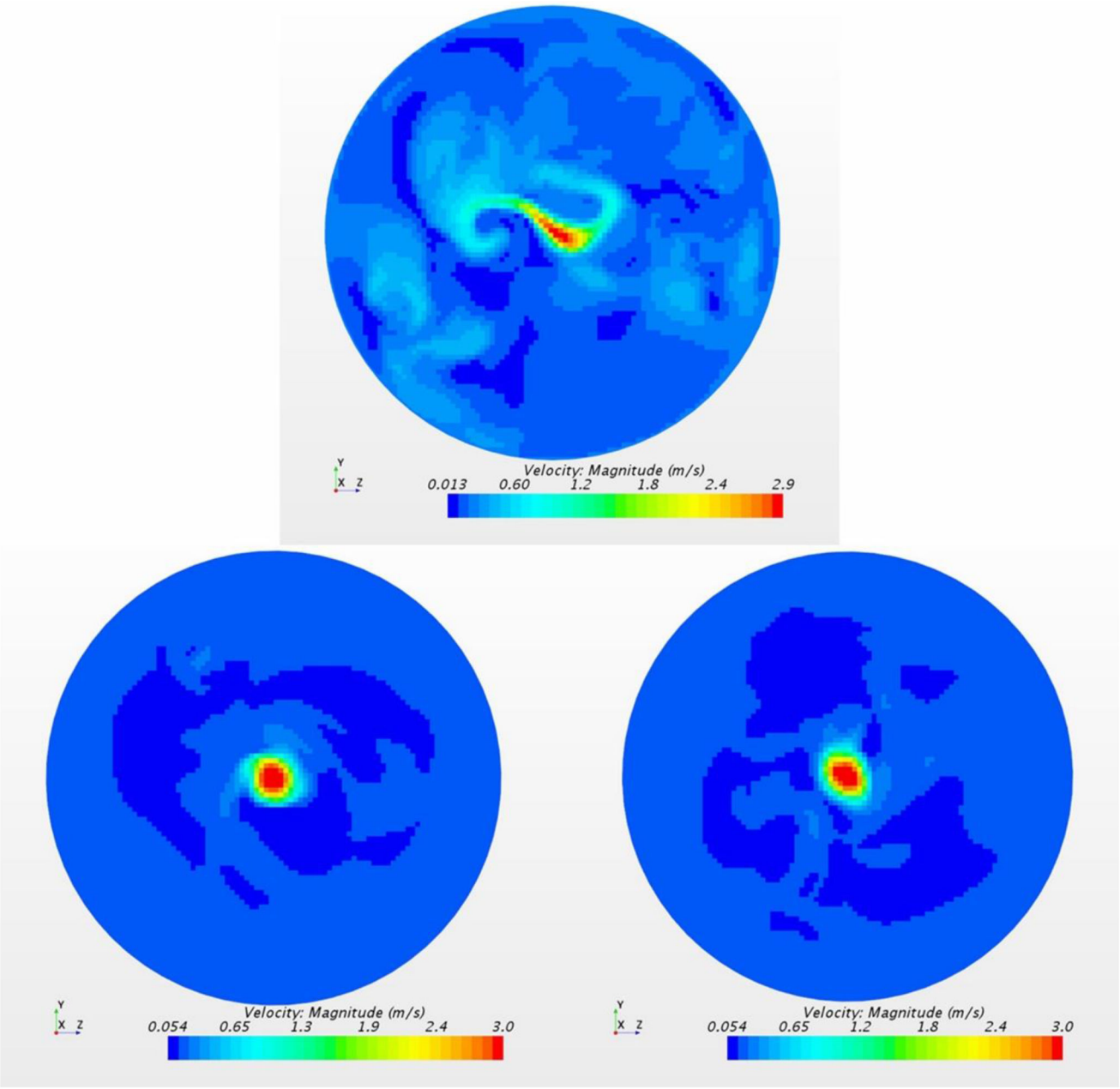

Figure 5b.

Air flow velocity magnitude (cloud image) at end plane (12.9 cm) of cylindrical drum (top: 90°; bottom left: 45° anti-clockwise; bottom right: 45° clockwise); t = 60 sec.

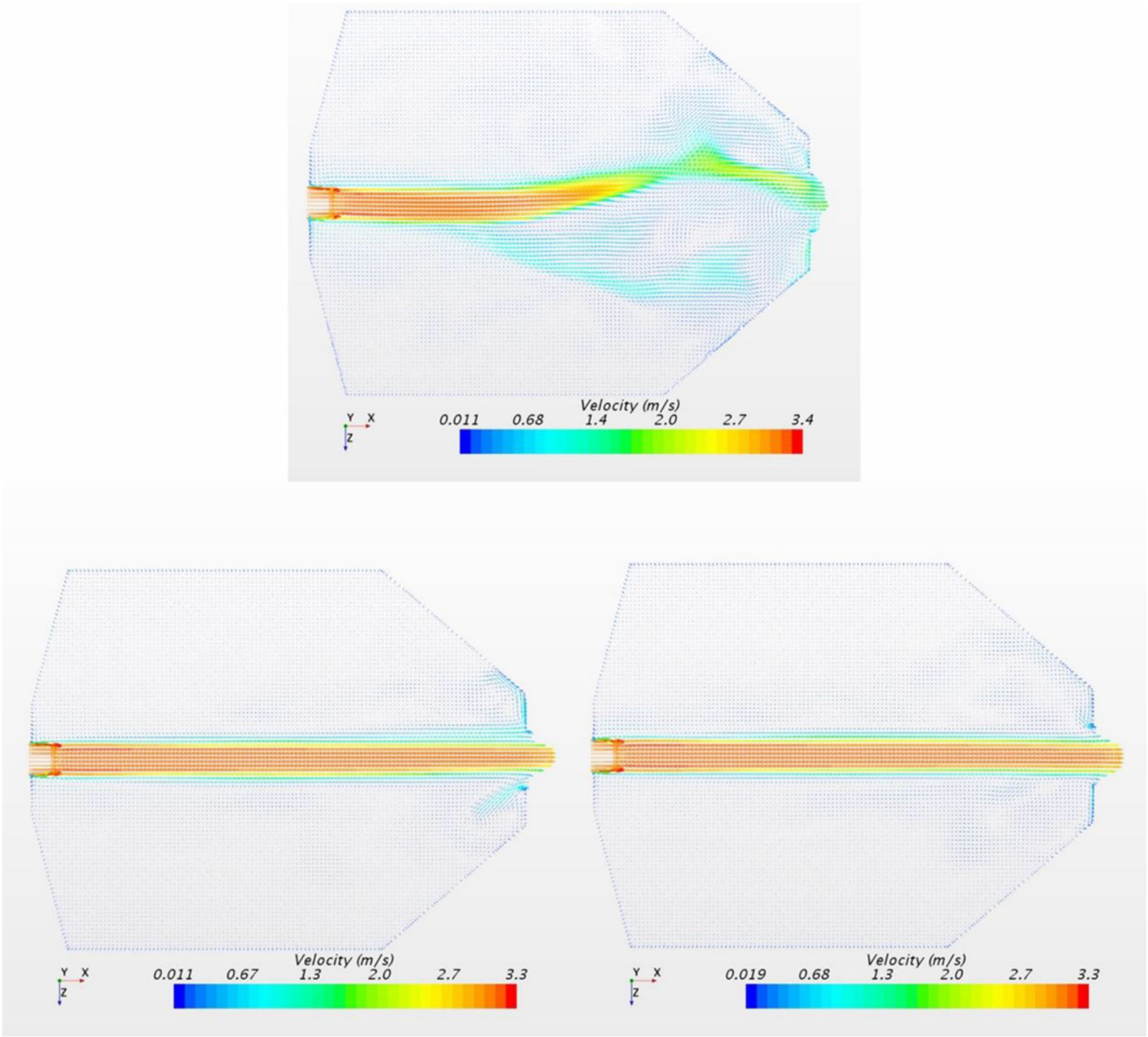

Figure 6a.

Air flow velocity vectors on central horizontal plane of cylindrical drum (top: 90o; bottom left: 45o anti-clockwise, bottom right: 45o clockwise); t = 30 sec.

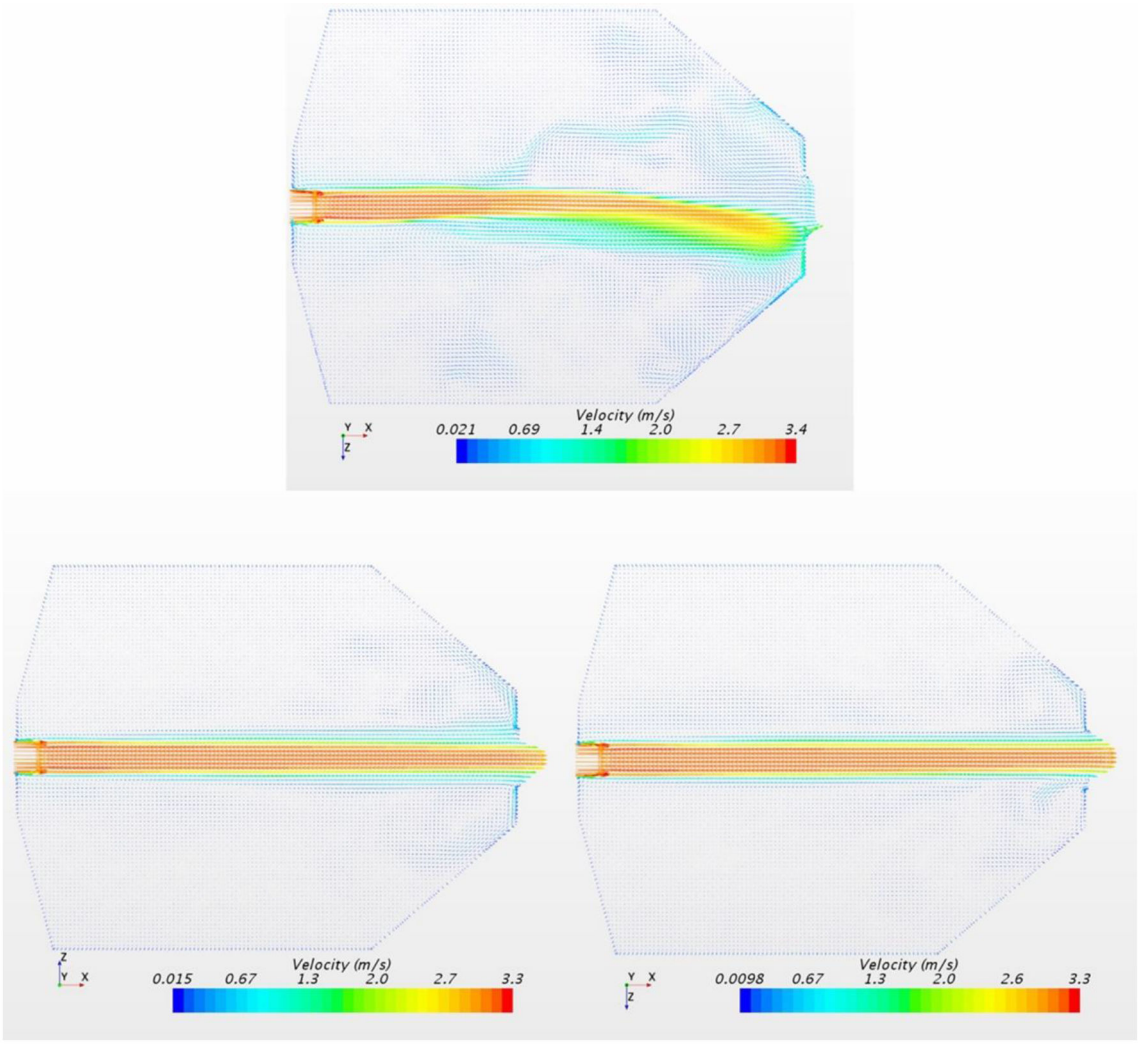

Figure 6b.

Air flow velocity vectors on central horizontal plane of cylindrical drum (top: 90o; bottom left: 45o anti-clockwise, bottom right: 45o clockwise); t = 60 sec.

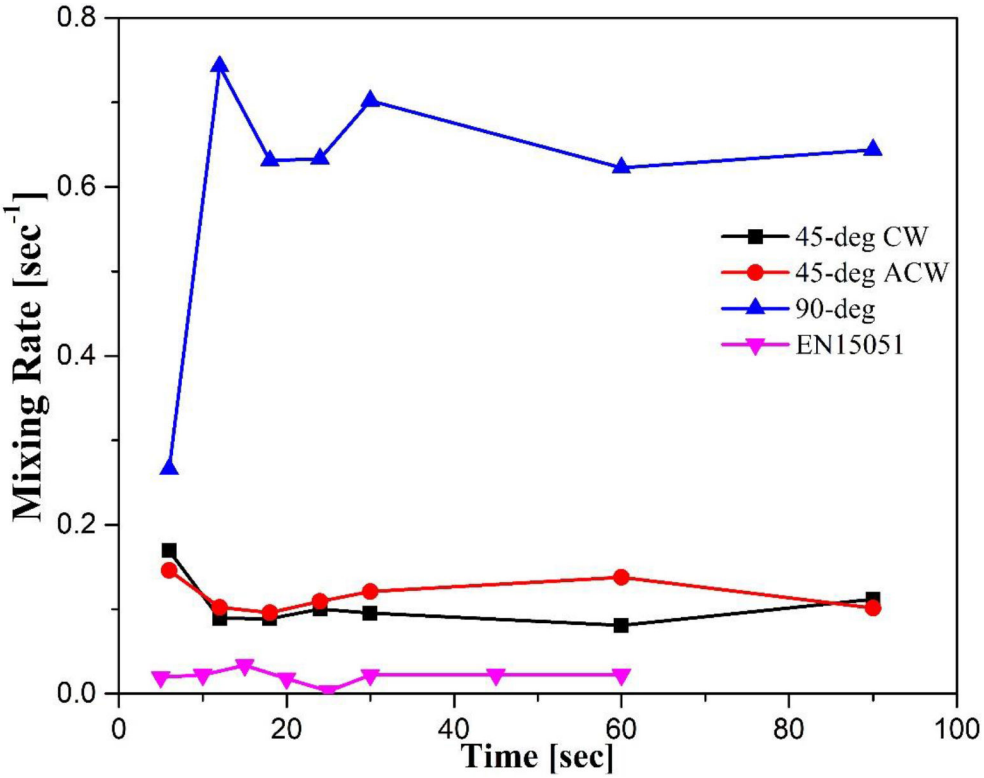

Figure 7.

Mixing Rate as a function of time at central plane of cylindrical drum (x = 0.083m for Heubach, x = 0.245 m for EN15051)

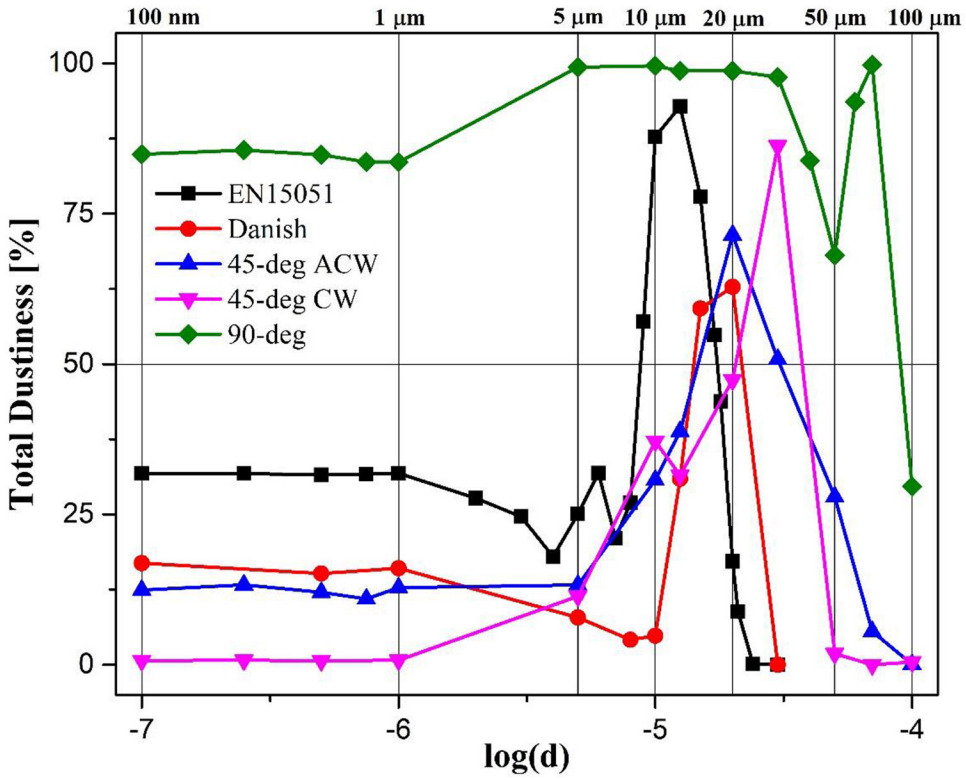

Figure 8.

Dustiness as a function of particle size for different rotating drums: Heubach 90° fins, 45° anticlockwise and clockwise fins; European Standard EN15051; small Danish drum. Particle size (absolute scale) indicated at top; $\log_{10}(d)$ at bottom, where diameter d is measured in meters.

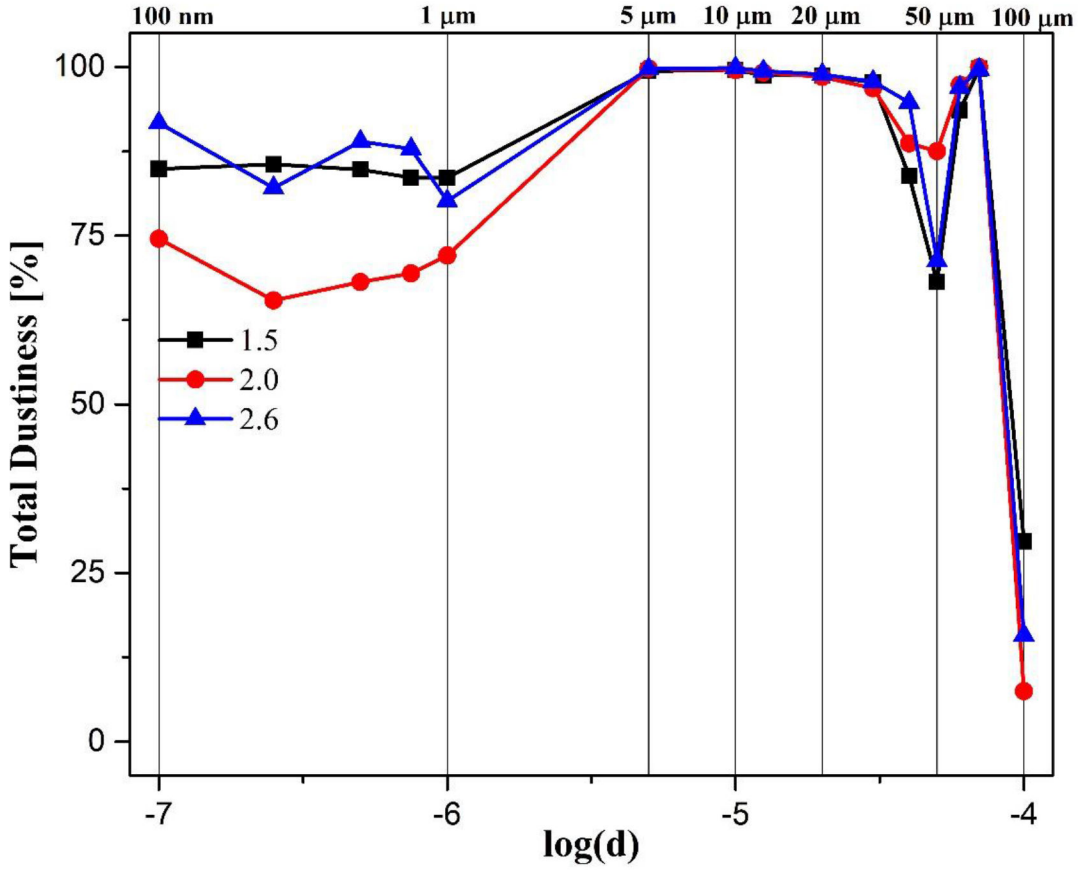

Figure 9.

Dustiness as a function of particle size for 90° Heubach drum; simulation results for different mesh sizes: 1.5 mm, 2.0 mm, 2.6 mm. Particle size (absolute scale) indicated at top; $\log_{10}(d)$ at bottom, where diameter d is measured in meters.

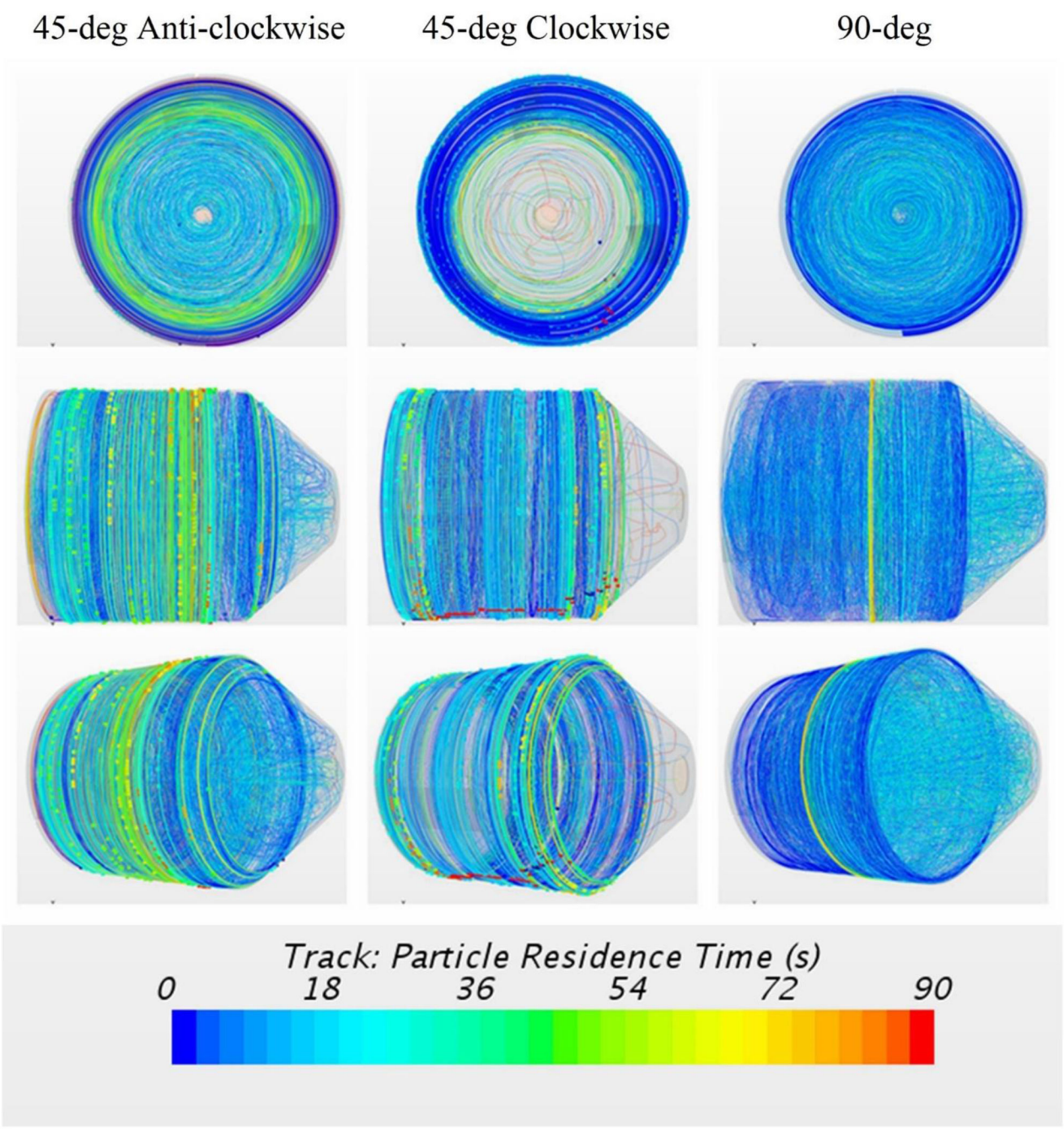

Figure 10.
Particle Track (d = 100 nm) in Heubach models. From left to right: 45° anti-clockwise, 45° clockwise, and 90°.

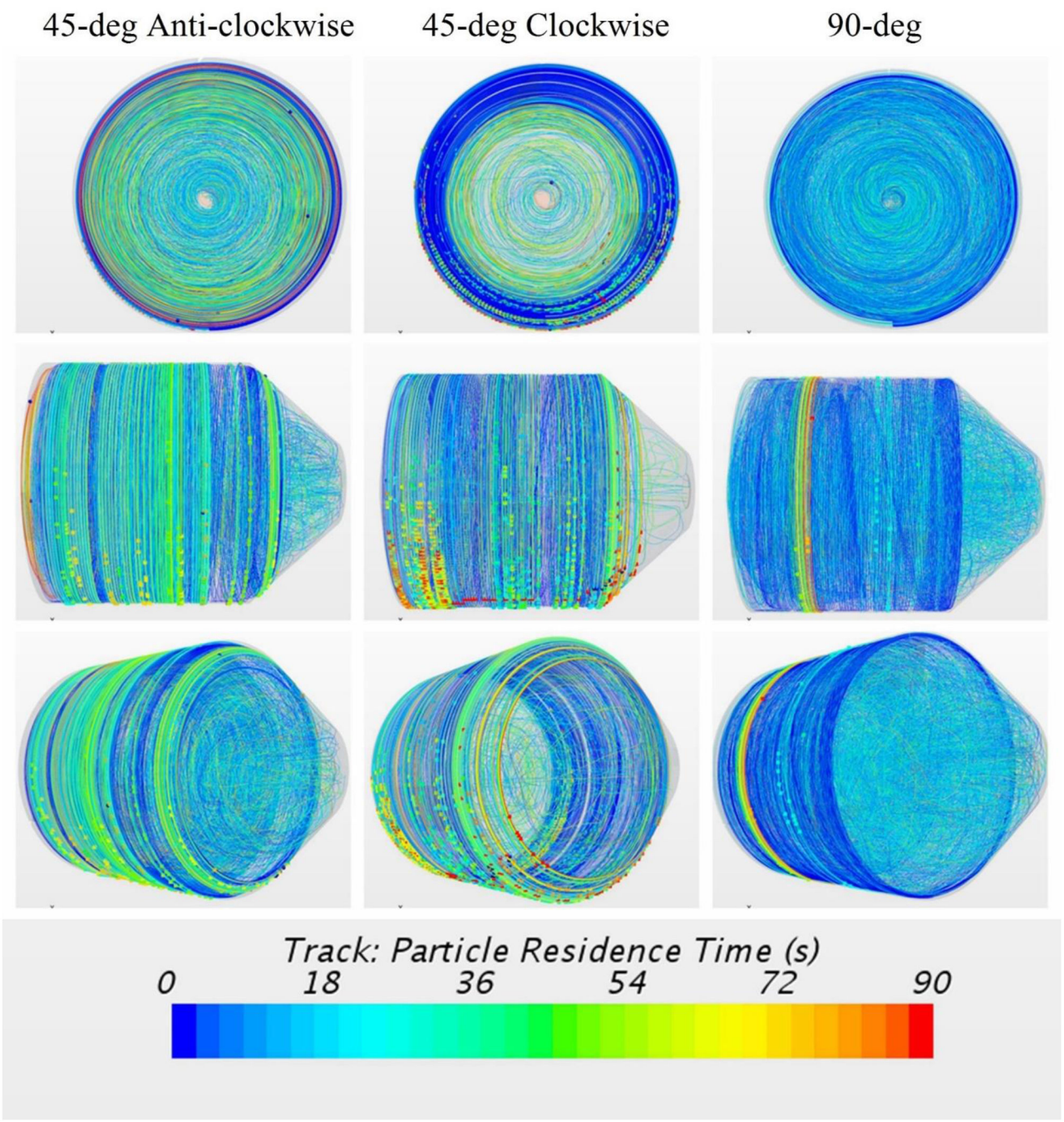

Figure 11.
Particle Track (d = 1 μm) in Heubach models. From left to right: 45° anti-clockwise, 45° clockwise, and 90°.

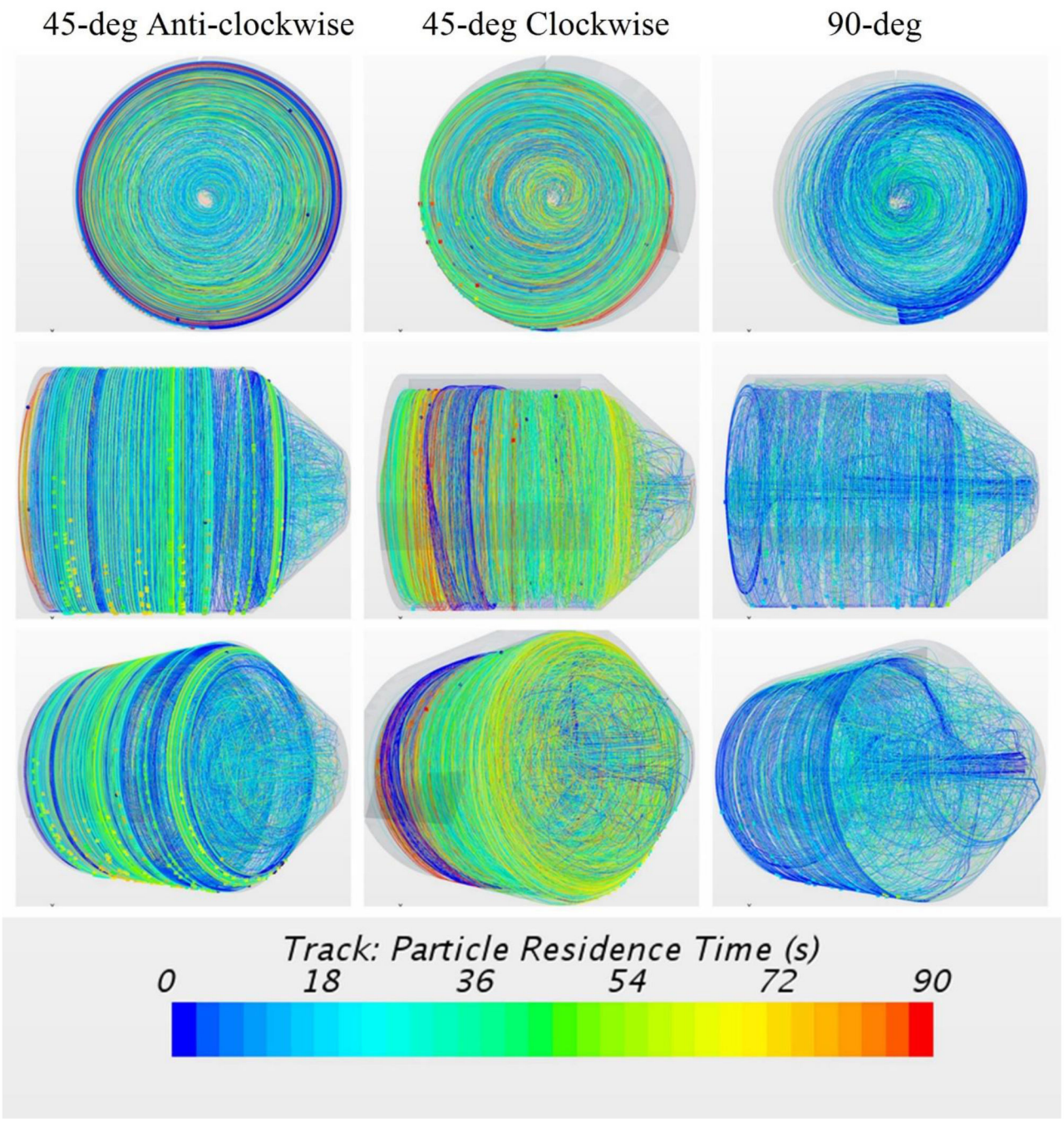

Figure 12.
Particle Track (d = 20 μm) in Heubach models. From left to right: 45° anti-clockwise, 45° clockwise, and 90°.

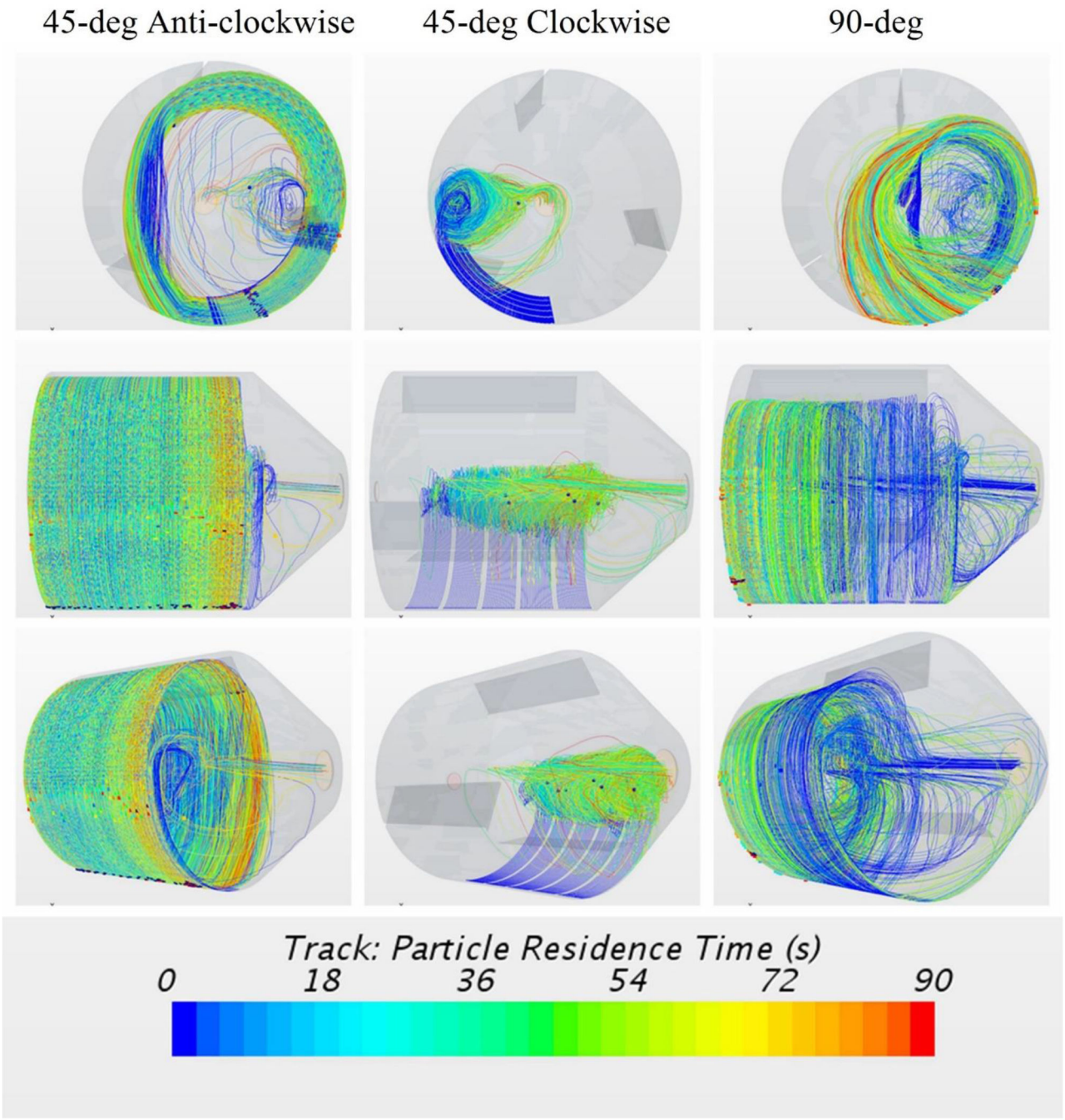

Figure 13.
Particle Track (d = 50 μm) in Heubach models. From left to right: 45° anti-clockwise, 45° clockwise, and 90°.

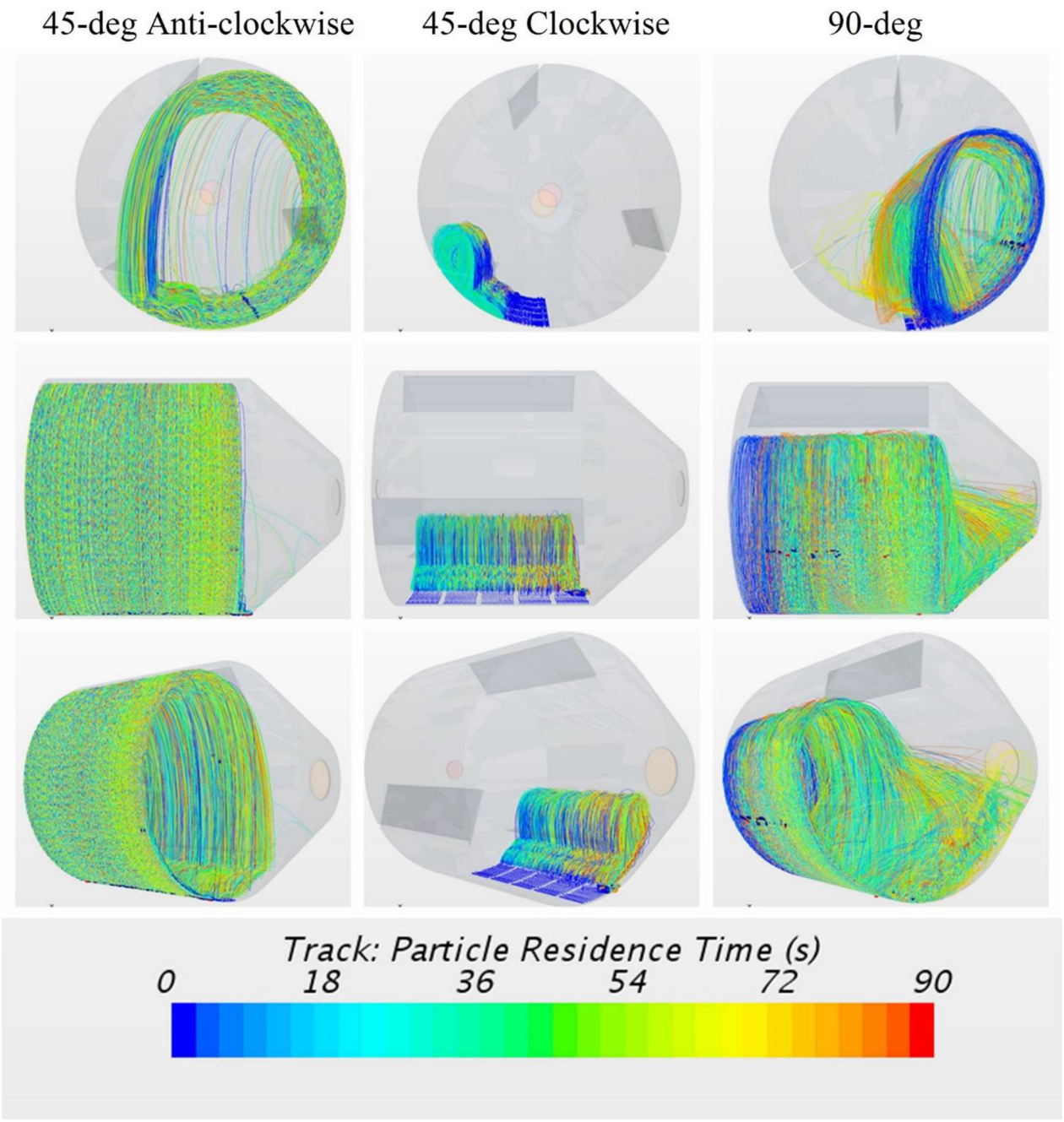

Figure 14.
Particle Track (d = 100 μm) in Heubach models. From left to right: 45° anti-clockwise, 45° clockwise, and 90°.

Table 1

Comparison of Parameters between EN15051 and Heubach Drums

	units	EN15051	Heubach
Inlet Diameter d_{in}	cm	15	1.2
Bulk Drum Diameter d_{bulk}	cm	30	14.0
Outlet Diameter d_{out}	cm	8	2.12
Inlet Length l_{in}	cm	13	1.4
Bulk Drum Length l_{bulk}	cm	23	11.5
Outlet Length l_{out}	cm	6	5.3
Volumetric Flow Rate Q	L/min	38	20
Angular Rotation Rate ω	rotations/min	4	30
Axial transit time $t_{transit}$	sec	32	5.4
$\omega\ t_{transit}$		2.2	2.7
Re_{in}		360	2300
Re_{bulk}		180	200
Re_{out}		670	1300
Re_{rot}		400	650

Table 2

Dimension Parameters Table of High-Speed Rotating Drum

Item	Unit	Quantity
Inlet Diameter	m	0.012
Outlet Diameter	m	0.0212412
Drum Diameter	m	0.14
Inlet Chamber Length	m	0.014
Outlet Chamber Length	m	0.053
Cylindrical Drum Chamber Length	m	0.115
Vane Count		3
Vane Height	m	0.025
Vane Length	m	0.119
Vane Thickness	m	0.001
Vane Angle	deg	45/90
Rotation Rate	rpm	30
Time Duration	second	300
Simulation Time	second	90

Table 3

Mesh Parameters for High-Speed Rotating Drum Simulations

Model	Heubach-45	Heubach-45	Heubach-90	Heubach-90	Heubach-90
Rotation Direction	Anti-Clockwise	Clockwise	Anti-Clockwise	Anti-Clockwise	Anti-Clockwise
Mesh Base Size [mm]	1.5	1.5	1.5	2	2.6
No. of Cells	920071	920071	859468	385986	384609
No. of Faces	2713561	2713561	2533338	1132683	1128732
No. of Vertices	921540	921540	863569	388387	387772

Table 4

Mesh parameters

Mesh Base Size [mm]	1.5	2	2.6
No. of Cells	859468	385986	384609
No. of Faces	2533338	1132683	1128732
No. of Vertices	863569	388387	387772